Open access • Journal Article • DOI:10.1007/S00126-015-0601-4

Metal-rich fluid inclusions provide new insights into unconformity-related U deposits (Athabasca Basin and Basement, Canada) — Source link

Antonin Richard, Michel Cathelineau, Marie-Christine Boiron, Julien Mercadier ...+2 more authors

Institutions: University of Lorraine, University of Leeds

Published on: 01 Feb 2016 - Mineralium Deposita (Springer Berlin Heidelberg)

Topics: Brine, Halite and Fluid inclusions

Article:
Richard, A, Cathelineau, M, Boiron, MC et al. (3 more authors) (2016) Metal-rich fluid inclusions provide new insights into unconformity-related U deposits (Athabasca Basin and Basement, Canada). Mineralium Deposita, 51 (2). pp. 249-270. ISSN 0026-4598

https://doi.org/10.1007/s00126-015-0601-4

Mineralium Deposita

Metal-rich fluid inclusions provide new insights into unconformity-related U deposits (Athabasca Basin and Basement, Canada)

--Manuscript Draft--

Manuscript Number:	MIDE-D-14-00078R3
Full Title:	Metal-rich fluid inclusions provide new insights into unconformity-related U deposits (Athabasca Basin and Basement, Canada)
Article Type:	Regular Articles
Corresponding Author:	Antonin Richard FRANCE
Corresponding Author Secondary Information:	
Corresponding Author's Institution:	
Corresponding Author's Secondary Institution:	
First Author:	Antonin Richard
First Author Secondary Information:	
Order of Authors:	Antonin Richard
	Michel Cathelineau
	Marie-Christine Boiron
	Julien Mercadier
	David Banks
	Michel Cuney
Order of Authors Secondary Information:	
Funding Information:	
Abstract:	The Paleoproterozoic Athabasca Basin (Canada) hosts numerous giant unconformity-related uranium deposits. The scope of this study is to establish the pressure, temperature and composition (P-T-X conditions) of the brines that circulated at the base of the Athabasca Basin and in its crystalline basement before, during and after UO2 deposition. These brines are commonly sampled as fluid inclusions in quartz- and dolomite-cementing veins and breccias associated with alteration and U mineralization. Microthermometry and laser ablation - inductively coupled plasma - mass spectrometry (LA-ICP-MS) data from five deposits (Rabbit Lake, P-Patch, Eagle Point, Millennium and Shea Creek) complement previously published data for the McArthur River deposit. In all of the deposits investigated, fluid inclusion salinity is between 25 and 40 wt.% NaCl equiv., with compositions displaying a continuum between a "NaCl-rich brine" end-member (Cl>Na>Ca>Mg>K) and a "CaCl2-rich brine" end-member (Cl>Ca≈Mg>Na>K). The CaCl2-rich brine has the highest salinity and shows evidence for halite saturation at the time of trapping. The continuum of compositions between the NaCl-rich brine and the CaCl2-rich brine end-members combined with P-T reconstructions suggest anisothermal mixing of the two brines (NaCl-rich brine : 180 ± 30°C and 800 ± 400 bars; CaCl2-rich brine: 120 ± 30°C and 600 ± 300 bars) that occurred under fluctuating pressure conditions (hydrostatic to supra-hydrostatic). However because the two brines were U-bearing and therefore oxidized, brine mixing was probably not the driving force for UO2 deposition. Several scenarios are put forward to account for the Cl-Na-Ca-Mg-K composition of the brines, involving combinations of seawater evaporation, halite dissolution, mixing with a halite-dissolution brine, Mg/Ca exchange during dolomitization, Na/Ca exchange by albitization of plagioclase, Na/K exchange by albitization of K-feldspar and Mg-loss by Mg-rich alteration. Finally, the metal concentrations in the NaCl-rich and CaCl2-rich

	brines are among the highest recorded compared to present-day sedimentary formation waters or fluid inclusions from basin-hosted base metal deposits (up to 600 ppm U, 3000 ppm Mn, 4000 ppm Zn, 6000 ppm Cu, 8000 ppm Pb and 10000 ppm Fe). The CaCl2-rich brine carries up to one order of magnitude more metal than the NaCl-rich brine. Though the exact origin of major cations and metals of the two brines remains uncertain, their contrasting compositions indicate that the two brines had distinct flow paths and fluid-rock interactions. Large-scale circulation of the brines in the Athabasca Basin and Basement was therefore a key parameter for metal mobility (including U) and formation unconformity-related U deposits.
Response to Reviewers:	Comments are included in the cover letter

Abstract

The Paleoproterozoic Athabasca Basin (Canada) hosts numerous giant unconformity-related uranium deposits. The scope of this study is to establish the pressure, temperature and composition (P-T-X conditions) of the brines that circulated at the base of the Athabasca Basin and in its crystalline basement before, during and after UO_2 deposition. These brines are commonly sampled as fluid inclusions in quartz- and dolomite-cementing veins and breccias associated with alteration and U mineralization. Microthermometry and laser ablation - inductively coupled plasma - mass spectrometry (LA-ICP-MS) data from five deposits (Rabbit Lake, P-Patch, Eagle Point, Millennium and Shea Creek) complement previously published data for the McArthur River deposit. In all of the deposits investigated, fluid inclusion salinity is between 25 and 40 wt.% NaCl equiv., with compositions displaying a continuum between a "NaCl-rich brine" end-member (Cl>Na>Ca>Mg>K) and a "$CaCl_2$-rich brine" end-member (Cl>Ca≈Mg>Na>K). The $CaCl_2$-rich brine has the highest salinity and shows evidence for halite saturation at the time of trapping. The continuum of compositions between the NaCl-rich brine and the $CaCl_2$-rich brine end-members combined with P-T reconstructions suggest anisothermal mixing of the two brines (NaCl-rich brine : 180 ± 30°C and 800 ± 400 bars; $CaCl_2$-rich brine: 120 ± 30°C and 600 ± 300 bars) that occurred under fluctuating pressure conditions (hydrostatic to supra-hydrostatic). However because the two brines were U-bearing and therefore oxidized, brine mixing was probably not the driving force for UO_2 deposition. Several scenarios are put forward to account for the Cl-Na-Ca-Mg-K composition of the brines, involving combinations of seawater evaporation, halite dissolution, mixing with a halite-dissolution brine, Mg/Ca exchange during dolomitization, Na/Ca exchange by albitization of plagioclase, Na/K exchange by albitization of K-feldspar and Mg-loss by Mg-rich alteration. Finally, the metal concentrations in the NaCl-rich and $CaCl_2$-rich brines are among the highest recorded compared to present-day sedimentary formation waters or fluid inclusions from basin-

hosted base metal deposits (up to 600 ppm U, 3000 ppm Mn, 4000 ppm Zn, 6000 ppm Cu, 8000 ppm Pb and 10000 ppm Fe). The $CaCl_2$-rich brine carries up to one order of magnitude more metal than the NaCl-rich brine. Though the exact origin of major cations and metals of the two brines remains uncertain, their contrasting compositions indicate that the two brines had distinct flow paths and fluid-rock interactions. Large-scale circulation of the brines in the Athabasca Basin and Basement was therefore a key parameter for metal mobility (including U) and formation unconformity-related U deposits.

Keywords

Brines - Metals - Fluid inclusions - Unconformity - Uranium - Athabasca

Introduction

The Athabasca Basin hosts numerous high-grade "unconformity-related" U deposits, located close to the interface between the crystalline basement, the sedimentary cover and basement-rooted faults. Most of the current models for their formation involve basin-derived oxidizing brines that were enriched in U through fluid-rock interaction and deposited the UO_2 at or close to the unconformity. Some authors (e.g. Hoeve and Sibbald 1978; Wilson and Kyser 1987) also invoke a basement-derived reducing fluid as being responsible for U reduction during mixing with basin-derived brines (see Jefferson et al. 2007; and Kyser and Cuney 2008, for reviews of genetic models). Because basin-derived brines are thought to be the uranium carrier, reconstructing their pressure, temperature and composition (P-T-X conditions) is crucial for understanding the origin of the world's richest U deposits. Bulk salinities, halogen (Cl–Br–I) and noble gas (Ar–Kr–Xe) systematics, and the stable chlorine isotopic composition of fluid inclusions as well as the boron isotopic composition of tourmaline, together indicate that these brines originated from sub-aerial evaporation of seawater (Derome et al. 2005; Richard et al. 2011; 2014; Leisen et al. 2012; Mercadier et al. 2012). Experimental work coupled with synchrotron-XRF, XANES and LA-ICP-MS analysis of fluid inclusions have shown that the U was probably transported in the form of uranyl(VI) chloride complexes, under low pH conditions and at the highest concentrations recorded for crustal fluids so far (pH = 2.5 to 4.5; [U] = 0.1 to ~ 600 ppm; Richard et al., 2010, 2012, 2013a; Dargent et al. 2013).

Many aspects of the Athabasca basin-derived brines remain controversial: (i) the origin of major solutes (i.e. seawater evaporation and/or fluid-rock interaction; Richard et al. 2010; Mercadier et al. 2012); (ii) the source of U and other metals (i.e. basin vs. basement rocks; Fayek and Kyser, 1997; Annesley and Madore 1999; Hecht and Cuney, 2000; Mercadier et al., 2013); and (iii) their P-T conditions (i.e. various estimates in the 80-300°C and 500-1500 bar ranges; Pagel

1975a, 1975b; Kotzer and Kyser 1995; Derome et al. 2005; Alexandre et al. 2005; Mercadier et al. 2010; Richard et al. 2013b).

In the Athabasca Basin, the only well-constrained deposit from a fluid inclusion perspective is the McArthur River deposit (Pagel and Ahamdach 1995; Kotzer and Kyser 1995; Derome et al. 2003, 2005; Richard et al. 2010, 2011, 2012, 2013a). Based on microthermometry, Raman spectroscopy and laser-induced breakdown spectroscopy (LIBS) analysis, Derome et al. (2005) concluded that a NaCl-rich brine had circulated at 220 ± 30°C and 1350 ± 150 bars, and a $CaCl_2$-rich brine had circulated at 110 ± 30°C and 700 ± 200 bars. Mixing between the two brines occurred during the pre-ore stage at 700 ± 200 bars after a pressure decrease from lithostatic to near hydrostatic conditions at 5-6 km depth. Using LA-ICP-MS analysis, detailed Na-Ca-Mg-K-Sr-Ba-U compositions of fluid inclusions were obtained that showed well-defined mixing trends between the NaCl-rich brine and the $CaCl_2$-rich brine end-members (Richard et al. 2010). In order to establish which characteristics of the McArthur River fluid inclusions could or could not be extrapolated to the entire Athabasca system, a microthermometric and LA-ICP-MS study of fluid inclusions was carried out on five deposits (Rabbit Lake, Shea Creek, Eagle Point, P-Patch and Millennium) located in various parts of the basin and above and below the unconformity.

Geology and sampling

Regional geology

The Athabasca Basin (Fig. 1a) unconformably overlies the Archean to Paleoproterozoic Western Churchill Province, which is separated into two subprovinces (the Rae Subprovince in the west and the Hearne Subprovince in the east) by the northeast-trending Snowbird tectonic zone (Hoffman 1990; Card et al. 2007; Jefferson et al. 2007). These two subprovinces consist of Archean gneisses,

Paleoproterozoic metapelites and mafic to felsic intrusions and were affected by the ~2.0 to ~1.9 Ga Thelon-Talston and the ~1.9 to ~1.8 Ga Trans-Hudson orogenies, respectively (Chiarenzelli et al. 1998; Annesley et al. 2005). The majority of the known unconformity-related U deposits in the Athabasca Basin are located close to the transition between two lithostructural domains of the Hearne Subprovince, known as the Wollaston-Mudjatik transition zone (WMTZ), which consists of a northeast-trending, anastomosing structure of Hudsonian age (1.8 Ga) (Annesley et al. 2005).

The sedimentary sequence of the Athabasca Basin (the Athabasca Group) was deposited from about 1.75 Ga onwards (Ramaekers et al. 2007). The current maximum thickness of the sedimentary cover is ~1.5 km and could have reached around 5 km according to P-T estimates from fluid inclusions (Pagel, 1975a, 1975b; Derome et al. 2005). From the base to the top, the Athabasca Group is composed of fluvial to marginal marine quartz-rich sandstones (Fair Point, Read, Smart and Manitou Falls formations), marine sandstones, phosphatic siltstones and phosphatic mudstones (Lazenby Lake and Wolverine Point Formations), sandstones (Locker Lake and Otherside Formations), shales (Douglas formation) and finally stromatolitic carbonates (Carswell formation) (Ramaekers et al. 2007). The Douglas and Carswell formations are only preserved around the Carswell meteorite impact structure (Pagel et al. 1985; Genest et al. 2010).

Unconformity-related U deposits

The U deposits are generally located near the basement/cover interface and are structurally controlled by sub-vertical faults rooted in graphite-rich basement metapelites. The spatial distribution of the ore and alteration minerals around the unconformity varies greatly between the deposits. The UO_2 ores may be basement-hosted (e.g. P-Patch, Eagle Point and Millennium), unconformity-hosted (e.g. McArthur River, Rabbit Lake) or sandstone-hosted (e.g. Cigar Lake), sometimes within the same deposit (e.g. Shea Creek).

131 The earliest UO_2 ores in the Athabasca Basin have been dated to between 1.6 and 1.4 Ga and
132 successive late episodes of recrystallization occurred until ~ 0.7 Ga (Cummings and Krstic 1992;
133 Fayek et al. 2002; Alexandre et al. 2009; Alexandre et al. 2012). Remobilization of primary UO_2 by
134 meteoric fluids along roll-fronts in basement rocks likely occurred from around 400 Ma and
135 continued to recent times (Wilson et al. 1987; Kotzer and Kyser 1995; Mercadier et al. 2011a).
136 Alteration occurs on a large-scale in the Athabasca basin but is most extensively developed
137 around the U-ores (Earle and Sopuck 1989; Quirt 2003). The main features include: (i) partial to
138 complete replacement of the initial basement minerals (K-feldspar, biotite, plagioclase, hornblende)
139 by an illite + sudoite (Mg-chlorite) ± dravite (Mg-tourmaline) assemblage (e.g. Alexandre et al.
140 2005; Mercadier et al. 2010), as well as the precipitation of quartz, illite and sudoite in the
141 sandstone porosity (Kotzer and Kyser 1995; Lorilleux et al. 2002; Derome et al. 2005; Kister et al.
142 2006); (ii) quartz dissolution in basement rocks as well as in the sandstones (e.g. Lorilleux et al.
143 2003; Mercadier et al. 2010); (iii) precipitation of UO_2 in the alteration- and quartz dissolution-
144 related porosity, as well as in veins and breccias (dravite + quartz ± dolomite ± bitumen also being
145 found as cements in these mineralized or barren structures; e.g. Hoeve and Sibbald 1978; Derome et
146 al. 2005); and (iv) rare earth element mobilization and redistribution among aluminium phosphate-
147 sulphate minerals and UO_2 (e.g. Fayek and Kyser 1997; Gaboreau et al. 2007; Mercadier et al.
148 2011b).
149
150 Fluid inclusion nomenclature and previous studies
151
152 In this study, we use the fluid inclusion nomenclature defined by Derome et al. (2005) for the
153 McArthur River deposit. Five fluid-inclusion types are defined on the basis of their
154 microthermometric characteristics. Inclusions with a halite cube at room temperature are termed
155 Lwh' or Lwh according to the last phase (ice or hydrohalite, respectively) to melt at low

156 temperature and to the mode of homogenization (by halite or vapor disappearance, respectively) at
157 high temperature. Inclusions that contained no halite cubes and whose last phase to melt at low
158 temperature was hydrohalite, are noted Lw2. Inclusions that contained no halite cube and whose last
159 phase to melt at low temperature was ice are noted Lw' (-60°C < Tm ice < -30°C), Lw1 (-30°C <
160 Tm ice < -15°C), or Lw'' (-15°C < Tm ice < 0°C), where Tm ice is the temperature of ice-melting.
161 Lw' and Lwh' inclusions frequently failed to nucleate ice during during cooling, even at
162 temperatures as low as -190°C (about a third of these inclusions), preventing observation of first
163 melting (Te) and ice melting (Tm ice). Previous LIBS and LA-ICP-MS analyses of McArthur River
164 fluid inclusions have shown that Lw1, Lw2 and Lwh inclusions are more representative of the
165 NaCl-rich brine, whereas Lw' and Lwh' are more representative of the $CaCl_2$-rich brine (Derome et
166 al., 2005; Richard et al., 2010). Lw'' inclusions were classified as late "low salinity fluids" by
167 Derome et al. (2005) and are unrelated to NaCl-rich and $CaCl_2$-rich brines.

168 Previous fluid inclusion data for the McArthur River deposit are summarized in Table 1
169 (Derome et al. 2005; Richard et al. 2010) and show the contrasting compositions and
170 microthermometric characteristics of fluid inclusions representative of the NaCl-rich brine (Lw1,
171 Lw2, Lwh) and $CaCl_2$-rich brine (Lw', Lwh'). Previous microthermometric data from the
172 Athabasca Basin were compiled and fluid inclusions were tentatively classified according to the
173 nomenclature used in this study (Table 2). Some fluid-inclusion types are widely represented across
174 the previously studied areas (Lw1, Lwh, Lwh''), while others are more scarce (Lw2, Lw'). This
175 could be due to the difficulties in observing hydrohalite melting in Lw2 inclusions and to the fact
176 that Lw' inclusions frequently fail to nucleate ice upon cooling, which may have limited the
177 reporting of microthermometric data for such fluid inclusions. However, this compilation does show
178 that fluid inclusions representative of the NaCl-rich brine (Lw1, Lw2, Lwh) and $CaCl_2$-rich brine
179 (Lw', Lwh') have been described in most of the deposits, as well as in unmineralized central parts
180 of the basin (Rumpel Lake).

181

182 Quartz and dolomite and their fluid inclusions in the ore-forming process

183

184 It is generally agreed that quartz is spatially closely-associated with the main alteration minerals
185 (illite, sudoite, dravite) and UO_2 (Dahlkamp 1978; Hoeve and Sibbald 1978; Wilson and Kyser
186 1987; Kotzer and Kyser 1995; Fayek and Kyser 1997; Kyser et al. 2000; Lorilleux et al. 2002;
187 Derome et al. 2005; Kyser and Cuney 2008; Ng et al. 2013). Furthermore, carbonates (calcite,
188 siderite and dolomite) are common in the Rabbit Lake, Shea Creek, Eagle Point and McArthur
189 River deposits (Hoeve and Sibbald 1978; Pagel et al. 1980; Hoeve et al. 1986; Heine 1986;
190 Lorilleux et al. 2002; Derome et al. 2005; Cloutier et al. 2011). Cross-cutting relationships suggest
191 that quartz and dolomite (the only carbonate studied here) cannot be placed in a single position
192 relative to UO_2 ore. For example, quartz has been variably interpreted as pre-ore (Ng et al. 2013),
193 pre- to post-ore (Dahlkamp 1978; Hoeve and Sibbald 1978; Derome et al. 2005), syn-ore (Kotzer et
194 al. 1992; Kotzer and Kyser 1995; Lorilleux et al. 2002) and post-ore (Alexandre et al. 2005;
195 Cloutier et al. 2009). Dolomite mainly occurs in the basement and, when found in the same mineral
196 assemblage, generally postdates associated quartz (Hoeve and Sibbald 1978; Derome et al. 2005).
197 The relative timings of the growth of alteration minerals (illite, sudoite, dravite), quartz, dolomite
198 and UO_2 can be difficult to ascertain because: (i) mineral deposition is often cyclic (Dahlkamp
199 1978; Hoeve and Sibbald 1978); (ii) the different stages are variably expressed in basement and
200 sandstone lithologies (Kyser and Cuney 2008; Alexandre et al. 2009); and (iii) recurrent episodes of
201 quartz dissolution may have occurred (Derome et al. 2005).

202 Consequently, it is always debatable as to whether a given sample contains fluid inclusions
203 which are fully representative of the fluids involved at the main UO_2 stage. However, all fluid
204 inclusion studies point to NaCl-rich and $CaCl_2$-rich brines as the uranium carrier and dominant fluid
205 involved from the pre-ore, syn-ore to the post-ore stages: (i) sandstone silicifications, which is

206 unanimously recognized as preceding the main UO_2 stage, show primary NaCl-rich and $CaCl_2$-rich
207 brine inclusions at the Cluff Lake and McArthur River deposits (Table 2, Pagel 1975a, 1975b;
208 Kotzer and Kyser 1995; Derome et al. 2005); (ii) the increasing intensity of illite-sudoite-dravite
209 alteration is related to an increasing abundance of secondary NaCl-rich and $CaCl_2$-rich brine
210 inclusion planes in magmatic and metamorphic quartz from basement rocks at the P-Patch deposit
211 (Mercadier et al. 2010); (iii) pre- to post-ore quartz in barren and mineralized samples contain
212 primary and pseudosecondary NaCl-rich and $CaCl_2$-rich brine inclusions (Pagel et al. 1980; Kotzer
213 and Kyser 1995; Derome et al. 2005); (iv) the O isotopic composition of quartz shows that quartz-
214 forming fluids (i.e. NaCl-rich and $CaCl_2$-rich brines) are isotopically equilibrated with illite, sudoite
215 and dravite (Richard et al. 2013b); (v) halogen and noble gas systematics of NaCl-rich and $CaCl_2$-
216 rich brine inclusions in quartz and dolomite and the B isotopic composition of dravite indicate a
217 common evaporated seawater origin for the NaCl-rich and $CaCl_2$-rich brines and the dravite-
218 forming fluids (Richard et al. 2011, 2014; Leisen et al. 2012; Mercadier et al. 2012); and (vi) LA-
219 ICP-MS analysis of NaCl-rich and $CaCl_2$-rich brine inclusions in pre- to post-ore quartz and the
220 inclusions were found to contain up to 600 ppm U (Richard et al. 2010, 2012) and Synchrotron-
221 XRF and XANES analyses in NaCl-rich brine inclusions showed that the uranium was in the
222 oxidized form, U(VI) (Richard et al. 2013a).
223
224 Sampling strategy
225
226 Because of the close association between the quartz, dolomite, alteration minerals and the UO_2,
227 quartz and dolomite cements in veins and breccias were targeted as potentially hosting fluid
228 inclusions that are representative of the dominant fluid involved at the time of alteration and
229 mineralization.

Five uranium deposits from the Athabasca Basin were sampled for this study (Rabbit Lake, Shea Creek, P-Patch, Millennium and Eagle Point) and previously published data from the McArthur River deposit (P2 North orebody) were used for comparison (Derome et al. 2005; Richard et al. 2010), covering various mineralized areas in the basin (Fig. 1a). These deposits share the typical characteristics of unconformity-related U deposits described above.

Sampling focused on basement-hosted mineralization and alteration, largely because of a lack of preserved sedimentary cover (Rabbit Lake and Eagle Point) and lack of sandstone-hosted quartz and dolomite cements in veins or breccias (P-Patch and Millennium). Four samples that exhibited quartz cementing veins were selected in sandstones at Shea Creek (IF23, IF29, IF41, IF98), 20 to 30 m above the unconformity. For basement-hosted samples (33 quartz and 14 dolomite samples), the depth below the unconformity ranges from 13 m (EPE44-17, Eagle Point) to 361 m (EPE44-14, Eagle Point). A brief petrographic description of the samples is given in Electronic Supplementary Materials (ESM 1). Figure 2 illustrates some of the typical quartz and dolomite occurrences studied in this work.

The selected quartz and dolomite samples cement veins and breccias hosted by unaltered to strongly altered (illite-sudoite-dravite) rocks. Based on previous work on the McArthur River deposit only barren samples were selected for analysis: (i) water radiolysis around UO_2 ores can lead to enrichment in H_2 and O_2 causing abnormally high homogenization temperatures of fluid inclusions (Derome et al. 2003, 2005); (ii) mineralized samples can be problematic during LA-ICP-MS analysis because of the potential for surface contamination and the presence of U-rich quartz domains (Richard et al. 2010); and (iii) fluid inclusions with similar major and trace element contents have been found in both mineralized and barren samples (Derome et al. 2005; Richard et al. 2010).

255 Fluid inclusion petrography

256

257 Within the quartz and dolomite, the petrography of fluid inclusions is generally complex due to (i)
258 alternating quartz growth and dissolution episodes; and (ii) intense microfracturing during mineral
259 growth, leading to the formation of clusters of primary and pseudosecondary inclusions. Therefore,
260 the application of the fluid inclusion assemblage concept (Goldstein and Reynolds 1994) is difficult
261 in this context. These processes are recurrent throughout the formation of millimetre-sized quartz
262 and dolomite, and primary and pseudosecondary inclusions could only be clearly distinguished
263 from one another in rare cases (Fig. 2). Therefore, the inclusions analyzed are considered to be
264 representative of a single fluid event associated with the filling of veins and breccias.

265 Two-phase (liquid-vapor) or three-phase (liquid-vapor-halite) fluid inclusions, 5 to 25 µm in
266 size, are typically observed in both quartz and dolomite (Fig. 2). The volumetric proportion of the
267 vapor phase is ~ 10%. Inclusions present negative crystal or more irregular shapes. A small number
268 of inclusions contain solids with the presence of hematite and/or phyllosilicates, all interpreted to be
269 daughter minerals due to their near constant volume relative to the volume of fluid inclusions.

270

271 **Methods**

272

273 Fluid inclusion microthermometry

274

275 Microthermometry was performed on fluid inclusions using a Linkam MDS600 heating-cooling
276 stage. The temperatures of phase changes were measured for the following: first melting (Te), ice
277 melting (Tm ice), hydrohalite melting (Tm hyd), halite dissolution (Ts NaCl) and homogenization
278 to the liquid phase (Th). The temperatures of phase changes have a precision of about ± 5°C for Te,
279 ± 0.1°C for Tm ice and Tm hyd, and ± 1°C for Ts NaCl and Th. The composition of fluid inclusions

was calculated in the two-salt NaCl-$CaCl_2$-H_2O system or single-salt NaCl-H_2O and $CaCl_2$-H_2O systems, using microthermometric data and numerical models based on empirical best-fits of phase equilibria determined from experimental data. When only Tm ice was observed, fluid inclusion composition could only be calculated in single-salt systems NaCl-H_2O (Lw1 inclusions) or $CaCl_2$-H_2O (Lw´ inclusions) using the AqSo2 computer program (Bakker 2003). When at least two phase transitions were observed, the fluid inclusion composition was calculated in the NaCl-$CaCl_2$-H_2O system using Tm ice - Tm hyd pairs (Lw2 inclusions) or Tm ice - Ts NaCl pairs (Lwh and Lwh´ inclusions), using Steele-MacInnis et al. (2011). Isochores have been drawn on the basis of the mean salt content and the Th modes of the fluid inclusions using the FLUIDS 1 package (Bakker 2003) and the equations of Zhang and Frantz (1987).

LA-ICP-MS analysis of fluid inclusions

166 fluid inclusions from 9 quartz samples from the Rabbit Lake, P-Patch, Eagle Point and Millennium deposits, containing both NaCl-rich and $CaCl_2$-rich brine inclusions, were selected (ESM 1). LA-ICP-MS analysis of fluid inclusions was carried out at the School of Earth and Environment, University of Leeds, at instrumental conditions reported in Allan et al. (2005). Individual quartz-hosted fluid inclusions were ablated with a ArF 193 nm Geolas Q Plus excimer laser (Microlas, Göttingen, Germany). Ablation took place in an He atmosphere and the ablated material was transported by a 0.68-ml/min He flow to a mixing device where 1 $l.min^{-1}$ Ar was added. Ablated samples were subsequently analyzed in an Agilent 7500c Quadrupole ICP-MS equipped with an Octopole Reaction System. The analyses were run with the reaction cell pressurized with 2.5 $ml.min^{-1}$ H_2 in order to eliminate $^{40}Ar^+$ and $^{40}Ar^{16}O^+$ interferences on $^{40}Ca^+$ and $^{56}Fe^+$ and to reduce the high Ar-based backgrounds on $^{39}K^+$. The following elements were recorded: ^{7}Li, ^{23}Na, ^{24}Mg, ^{39}K, ^{40}Ca, ^{55}Mn, ^{56}Fe, ^{63}Cu, ^{66}Zn, ^{88}Sr, ^{137}Ba, ^{208}Pb and ^{238}U.

In all cases, ^{23}Na was used as internal reference element. Limits of detection (LODs) of the other elements were calculated using the 3σ criterion (Longerich et al. 1996). The analytical precision of most elements is within 15% RSD. For K, the analytical precision is better than 15% RSD. The analytical precision of the other elements is typically better than 30% RSD (Allan et al. 2005).

Calibration and signal-integration were performed with the Matlab®-based SILLS program (Guillong et al. 2008). Absolute element concentrations can be calculated from analyzed ratios relative to Na if this concentration is known. The Na concentration can be obtained from the salinity estimated from microthermometry (in wt.% NaCl equiv.) using the charge-balance technique (Allan et al. 2005). This method corrects the modelled amount of Na (from the wt.% NaCl equiv.) for contributions from other chloride salts using the analyzed elemental ratios to Na. Based on microthermometric measurements (ESM 2) a chlorinity of 6.5 molal was attributed to all inclusions, which should over- or underestimate absolute concentrations by a maximum of 30% relative, but more generally around 10% (Derome et al. 2005). Absolute element concentrations are given in ppm (equivalent $\mu g.g^{-1}$) and the complete LA-ICP-MS dataset is presented in ESM 3.

Results

Fluid inclusion distribution among samples

The absolute and relative abundances of the different microthermometric types of fluid inclusion in all samples are given in ESM 1. Microthermometric data and fluid inclusion compositions in the H_2O-NaCl-$CaCl_2$ system are summarized in ESM 2. Some samples contained only Lw1, Lw2 and Lwh, and others only Lw' and Lwh', however the majority of samples contained all types in variable proportions. Low salinity Lw'' inclusions were found very sporadically (ESM 2) and may

represent relicts of late fluids, unrelated to the NaCl-rich and $CaCl_2$-rich brines (Derome et al. 2005). They are not discussed here. Quartz and dolomite have comparable fluid inclusion contents except for Lwh' inclusions, which were almost only found in quartz (only one observation in dolomite). No relationship was found between fluid inclusion content, alteration and the depth relative to unconformity of the sample.

Fluid inclusion composition in the H_2O-NaCl-$CaCl_2$ system

The compositions of individual fluid inclusions are plotted in the ternary H_2O-NaCl-$CaCl_2$ diagram in Figure 3. Quartz and dolomite-hosted fluid inclusions cannot be distinguished. All deposits contain both Na-dominated and Ca-dominated inclusions as well as inclusions of intermediate composition. Taken together, the composition of fluid inclusions displays a continuum between NaCl-rich brine (20-25 wt.% salts) and a $CaCl_2$-rich brine (25-40 wt.% salts) end-member.

The Te of Lw1 inclusions is generally between -60 and -55°C, and Tm ice is between -30°C and -15°C with most observed values around -25°C (ESM 2). In the H_2O-NaCl-$CaCl_2$ system, Tm hyd can be higher or lower than Tm ice, and Tm ice - Tm hyd pairs are indicative of Na/Ca ratios. The case where Tm hyd is higher than Tm ice is typically represented by Lw2 inclusions (see below). Alternatively, if Tm hyd is lower than Tm ice, this would result in a wide range of possible Na/Ca ratios and possibly Ca-dominated compositions. In practice, the observation of hydrohalite melting before ice melting is complicated by the difficulty in distinguishing ice from hydrohalite when the two phases are mixed. Attempts to use sequential freezing to coarsen hydrohalite to observable sizes before ice melting (Haynes et al. 1985) were unsuccessful. Lw1 inclusions are therefore suspected to be metastable Lw2 inclusions that failed to nucleate any hydrohalite during cooling.

In Lw2 inclusions, Te is generally between -60 and -55°C and hydrohalite is the last phase to melt. Tm ice is centred on -25°C and Tm hyd between -21°C and +21°C (ESM 2). In the H_2O-NaCl-$CaCl_2$ system, hydrohalite melting is limited to the -21.0 to -0.1°C range. Here, positive Tm hyd indicates either stable hydrohalite melting in a more complex solution or metastable hydrohalite melting (Zwart and Touret 1994). Repeated measurements showed that Tm hyd were reproducible to within ± 1°C. Therefore, we consider positive Tm hyd to be the consequence of complex chemistry of the solutions. Although a wide range of molar Na/Ca ratios were calculated in Lw2 inclusions, most values centre on the 3-4 range.

Lwh inclusions generally have Te between -60 and -55°C. Tm ice is generally between -40 and -25°C and Tm hyd is observed in the majority of inclusions and is between -20 and +21°C (ESM 2). Ts NaCl is between 81 and 208°C. As for Lw2 inclusions, positive Tm hyd may indicate a complex chemistry of the solutions. Lwh inclusions have calculated Na/Ca ratios close to 5.

For about a third of Lw' inclusions, ice melting is not frequently observed due to the fact that fluid inclusions failed to nucleate ice during cooling, even at temperatures as low as -190°C. When ice formed, Te is between -70 and -60°C and Tm ice is between -55 and -30°C (ESM 2). These low Te and Tm ice values indicate a complex chemistry. As for Lw1 inclusions, hydrohalite melting theoretically occurs before ice melting. Attempts to use sequential freezing to coarsen hydrohalite to observable sizes before ice melting (Haynes et al. 1985) were unsuccessful. The field for possible compositions of Lw' inclusions in the H_2O-NaCl-$CaCl_2$ system is delimited by the H_2O-$CaCl_2$ axis and the hydrohalite field and ice melting isotherms (-55°C and -30°C; Fig. 3b) and results in Na/Ca ratios ranging from to 0.3 to near zero.

Lwh' inclusions exhibit low temperature behaviour comparable to Lw' inclusions and ice failed to nucleate during cooling even down to -190°C for about a third of these inclusions. Te is between -70 and -60°C and Tm ice is generally between -55 and -30°C. Ts NaCl is between 99 and 260°C. Calculated molar Na/Ca ratios mostly range from 0.3 to 1 (ESM 2).

379 Tm ice - Th pairs

380

381 Figures 4 and 5 show the Tm ice - Th pairs for quartz-hosted and dolomite-hosted fluid inclusions,
382 respectively. The Th are highly variable and range from ~60°C to ~200°C for all fluid inclusion
383 types. For both hosts, the Tm ice forms a continuum between ~ -15 and ~ -60°C. Th is highly
384 variable (± 70°C) for every restricted range of Tm ice. For quartz-hosted inclusions, all deposits
385 show a majority of Tm ice values scattered around -25°C and less frequent Tm ice data below -
386 30°C. Note that for the later inclusions (Lw' and Lwh') Tm ice could not be systematically
387 reported. This might explain some of the gaps in the continuum between the lowest Tm ice data (~-
388 55°C) and the highest Tm ice values (~25°C) where fewer data could be acquired (P-Patch,
389 Millennium). For quartz-hosted inclusions, the majority of observed Tm ice - Th pairs indicate a
390 general decrease in Th with Tm ice (Fig. 4), with the two end-members being the NaCl-rich brine
391 (Tm ice = ~ -20 to -30°C and most Th values between 100 and 150°C) and the $CaCl_2$-rich brine
392 (Tm ice = ~ -50 to -60°C and most Th values of between 80 and 130°C). The only exception is the
393 NaCl-rich brine inclusions at McArthur River, which have a significantly the higher Th distribution
394 (most Th values between 120 and 170°C). A comparable trend of a general decrease in Th with Tm
395 ice could approximately fit the dolomite-hosted inclusion data (Fig. 5).

396

397 Ts NaCl - Th pairs

398

399 Figure 6a shows Ts NaCl - Th pairs for quartz and dolomite-hosted Lwh and Lwh' inclusions. Most
400 Lwh inclusions scatter close to the 1:1 slope whereas the majority of Lwh' inclusions scatter to the
401 right of the 1:1 slope. The temperature difference between Ts NaCl and Th is represented as Δ(Ts
402 NaCl - Th) and shows a continuum between -107°C and 216°C (Fig. 6b). While the volumetric
403 proportion of vapor phase is always close to 10% of the total fluid inclusion volume, the volume of

404 the NaCl phase shows the highest variability (up to twice the volume of the vapor phase).
405 Consequently, the Lwh and Lwh' inclusions have been classified as a function of the volumetric
406 relationship between NaCl and the vapor phase, into three groups: inclusions in which the volume
407 of the NaCl phase (V(NaCl)) is lower, equal or higher than the volume of the vapor phase (V(vap)).
408 Figure 6b shows that the highest Δ(Ts NaCl - Th) values are associated with fluid inclusions where
409 V(NaCl) > V(Vap), and conversely, the lowest Δ(Ts NaCl - Th) values are associated with fluid
410 inclusions where V(NaCl) < V(Vap).
411
412 Fluid inclusion compositions analyzed by LA-ICP-MS
413
414 A continuum of fluid inclusion compositions is observed between a low-Na end-member and a
415 high-Ca end-member (Fig. 7, ESM 3). This dataset cannot be fully representative of all the possible
416 compositions in each deposit due to the relatively small number of samples investigated (e.g. the
417 absence of Ca-rich compositions at Eagle Point). At the sample scale, although neither
418 microthermometry nor LA-ICP-MS analysis can be considered fully representative of the overall
419 fluid inclusion variability due to the relatively small number of inclusions analyzed, the distribution
420 of Na-dominated inclusions and Ca-dominated inclusions are consistent with the distribution seen
421 in microthermometry data (Fig. 3, 7; ESM 1, 3). While there may be some minor differences
422 between deposits, the continuum was observed in most localities. The LA-ICP-MS data will
423 therefore be described and discussed for all deposits together.
424 The proportions of fluid inclusions with element concentrations above the LOD are as
425 follows: Li (85%); Na (100%); Mg (100%); K (93%); Ca (100%); Mn (52%); Fe (94%); Cu (42%);
426 Zn (70%); Sr (99%); Ba (86%); Pb (82%) and U (63%). In inclusions in which the elements could
427 be quantified, the absolute content of every analyzed element is highly variable: Li = 40 to 16000
428 ppm; Na = 5400 to 140000 ppm; Mg = 590 to 53000 ppm; K = 930 to 52000 ppm; Ca = 640 to

429 96000 ppm; Mn = 38 to 2800 ppm; Fe = 32 to 16000 ppm; Cu = 2 to 6300 ppm; Zn = 6 to 4400; Sr
430 = 9 to 2800 ppm; Ba = 11 to 2100 ppm; Pb = 3 to 8100 ppm and U = 0.2 to 610 ppm (ESM 3).

431 Assuming that the high Na concentrations relate to the NaCl-rich brine and the low Na
432 concentrations relate to the $CaCl_2$-rich brine, it is possible to identify the likely composition range
433 for the NaCl-rich brine and $CaCl_2$-rich brine end-members. If Na concentrations of >80000 ppm
434 and <30000 ppm are representative of the NaCl-rich brine and $CaCl_2$-rich brine end-members,
435 respectively (Richard et al. 2010), the distributions of cation concentrations in each end-members
436 can be approached (Fig. 8). The $CaCl_2$-rich brine shows significant enrichment (up to one order of
437 magnitude) in Mg, K, Ca, Fe, Cu, Zn, Sr, Ba, Pb and U compared to the NaCl-rich brine (Fig. 8).
438 The NaCl-rich brine is characterized by Cl>Na>Ca>Mg>K brine whereas the $CaCl_2$-rich brine is a
439 Cl>Ca≈Mg>Na>K brine (Fig. 8). U concentration data have already been published and discussed
440 in detail in Richard et al. (2012).

441

442 **Discussion**

443

444 P-T-X conditions and scales for brine circulations

445

446 According to Ts NaCl - Th relationships and volumetric considerations on vapor and NaCl
447 phases (Fig. 6), the $CaCl_2$-rich brine was probably saturated with respect to halite at the time of
448 trapping (Becker et al. 2008). In this case, NaCl cubes would have been trapped heterogeneously
449 along quartz growth planes and fluid inclusions. During cooling to (sub)surface conditions after
450 trapping, the halite would either have nucleated within halite-free inclusions or coarsened from the
451 previously trapped NaCl nuclei. Given such a scenario, it is therefore possible that the Na
452 concentration in the $CaCl_2$-rich brine has been overestimated. Indeed, if NaCl crystals precipitated
453 in the hydrothermal solutions and were heterogeneously trapped within fluid inclusions

454 mechanically, then the compositions of the fluid inclusions may be richer in NaCl than the actual
455 composition of the brine. The causes of NaCl saturation at the time of trapping are uncertain. NaCl-
456 saturation can originate from (i) cooling of a high-temperature and high-salinity brine; (ii) salt
457 enrichment by H_2O uptake from brines to alteration minerals (Gleeson et al. 2003); or (iii) leaching
458 of Cl from Cl-bearing minerals. The first hypothesis cannot be completely excluded, however this
459 would imply trapping temperatures in excess of 250°C, which is above temperature estimates from
460 mineral thermometers in this context (Alexandre et al. 2005). The second and third hypotheses are
461 supported by the increase in the salinity of fluid inclusions, where alteration is most intense
462 (Mercadier et al. 2010), and the ~ 90% loss of Cl in altered rocks compared to their fresh
463 counterparts as a result of biotite breakdown (Richard et al. 2011). The influence of the last two
464 phenomena relies on the fluid-rock ratios, which to date remain poorly constrained.
465 The observed scatter of Th values observed in the Tm ice vs Th diagrams (Fig. 4) might be
466 explained by: (i) post-trapping reequilibration; (ii) partial leakage during heating; (iii) pressure
467 fluctuations during trapping; or (iv) heterogeneous contamination by trace gases. Post-trapping
468 reequilibration is commonly observed in diagenetic minerals (Goldstein 2001; Bodnar 2003). Such
469 modifications lead to changes in fluid inclusion density and variation of the volumetric fraction of
470 the vapor phase. Variation of the volumetric fraction of vapor phase within the range of the present
471 observations (< 10% relative) could lead to significant Th variation (several tens of degrees; Bodnar
472 2003). The 50-100°C variation in Th observed within some quartz-hosted and dolomite-hosted fluid
473 inclusion clusters supports this hypothesis. However, there is no clear optical evidence for post-
474 trapping re-equilibration. Partial leakage during heating frequently occurs in diagenetic minerals,
475 especially in carbonate cements (Goldstein and Reynolds 1994). It could well be that some of the
476 highest Th measured in dolomite have been affected by partial leakage, however there is no clear
477 optical evidence for this here. Pressure fluctuations between hydrostatic (lower limit) and supra-
478 hydrostatic regimes (upper limit) could account for around 40°C of Th variation if pressure varies

479 between purely hydrostatic and purely lithostatic (Dubessy et al. 2003). Pressure fluctuations in the
480 brines are predicted by seismic pumping (Behr et al. 1987). Over-pressuring (i.e. supra-hydrostatic
481 pressure) is also a common phenomenon in burial diagenesis (Swarbrick and Osborne 1997)
482 although a hydrostatic pressure regime appears to be the rule rather than the exception in the
483 Athabasca Basin (Cui et al. 2012a, 2012b; Chi et al. 2013). Contamination of fluid inclusions by
484 trace gases, even if not optically visible, is likely to lead to anomalously high Th. This hypothesis
485 has already been proposed for high Th values measured in the rare secondary low-salinity fluid
486 inclusions at McArthur River (Derome et al. 2005) and the detection of trace amounts of CO_2, CH_4,
487 H_2 and O_2 in brine inclusions by Raman spectroscopy was shown in Derome et al. (2003). Here, we
488 propose that gas contamination may have affected the two brines, possibly leading to the highest
489 measured Th (> 150°C).

490 On the basis of these assumptions, a reconstruction of P-T conditions for NaCl-rich and
491 $CaCl_2$-rich brines in unconformity-related deposits can be attempted. Isochores were drawn from
492 the most likely representative Th range for the two brine end-members in both quartz and dolomite:
493 80-130°C for the $CaCl_2$-rich brine and 100-150°C for the NaCl-rich brine (Fig. 9). Ts NaCl for
494 Lwh' inclusions were not taken into account because the $CaCl_2$-rich brine was saturated with
495 respect to halite at the time of trapping and only Th should represent the minimum trapping
496 temperature (Becker et al. 2008). The slopes of the isochores are slightly steeper for $CaCl_2$-rich
497 brines than for NaCl-rich brine inclusions due to their higher salinity. The P-T domain for trapping
498 is constrained by the isochores, the hydrostatic thermal gradient (lower limit) and the lithostatic
499 thermal gradient (upper limit). Note that in this model, static and reasonably low geothermal
500 gradients (30-40°C / km) are assumed, which is not always the case in fluid systems that show rapid
501 downflow or upflow as was possibly the case here (Bons et al. 2014). Therefore, such P-T
502 reconstruction should be considered with caution. From this, it can reasonably be deduced that the
503 $CaCl_2$-rich brine was trapped at 120 ± 30°C and 600 ± 300 bars and the NaCl-rich brine at 180 ±

504 30°C and 800 ± 400 bars (Fig. 9). Given that the depth below unconformity for the samples studied
505 is negligible compared to the thickness of the basin, the calculated past thickness of the Athabasca
506 Basin was ~ 3-6 km (Fig. 9). This P-T reconstruction is compatible with that of Derome et al.
507 (2005) based on McArthur River fluid inclusions. Our temperature estimate for the NaCl-rich brine
508 (180 ± 30°C) is compatible with independent thermometers based on illite and chlorite chemistry
509 and the oxygen isotope composition of quartz-tourmaline pairs, which generally give temperatures
510 of around 200°C (Kotzer and Kyser 1995; Ng et al. 2013). The estimated temperature of the $CaCl_2$-
511 rich brine (120 ± 30°C) however, differs significantly from that derived from the independent
512 thermometers. This could imply that the low temperature $CaCl_2$-rich brine was not recorded by the
513 independent geothermometers, i.e., it was not involved to any great extent in the alteration of illite-
514 sudoite-dravite. However, this does not mean that the low-temperature event was a late event. For
515 example, Derome et al. (2005) demonstrated that the low-temperature $CaCl_2$-rich brine was
516 responsible for pervasive sandstone silicification prior to the UO_2 stage and that higher temperature
517 NaCl-rich brine was also present before and after the UO_2 stage. The temperature difference
518 between the NaCl-rich and $CaCl_2$-rich brine might be explained by physical separation of the two
519 reservoirs. Derome et al. (2005) tentatively suggested that the cooler $CaCl_2$-rich brine originated
520 from the upper levels of the Athabasca Basin and percolated into the basement rocks without any
521 significant temperature re-equilibration, acquiring its Ca-rich composition before reaching deposit
522 sites. Although the occurrence of NaCl-rich brines and cooler $CaCl_2$-rich brines both originating
523 from seawater evaporation appears to be usual in Proterozoic basins (Boiron et al. 2010), this
524 temperature difference is far from fully understood and points out the need for further
525 hydrogeochemical modelling (Raffensperger and Garven 1995; Cui et al. 2012a, 2012b).

526 Finally, the overall continuity of microthermometric data and detailed compositions between
527 the NaCl-rich brine and the $CaCl_2$-rich brine end-members (Figs. 4, 5, 7) suggests that the data that
528 plot between the two end-members represent mixing terms. Moreover, the overall trend of a slight

529 decrease in Th from the NaCl-rich brine to the $CaCl_2$-rich brine end-members, as well as the P-T
530 reconstruction (Fig. 9), are in favor of anisothermal mixing between the two brines. Causes of
531 mixing of two physically-separated brine reservoirs could include the reactivation of basement-
532 rooted faults controlling alteration and mineralization on both sides of the unconformity and the
533 associated dense network of microfractures in basement rocks (Mercadier et al. 2010). Seismic
534 pumping could have driven brines from different reservoirs towards these fault zones (Behr et al.
535 1987). Although brine mixing was systematically associated with alteration and UO_2 deposition,
536 mixing itself could not have been the cause of reduction of U(VI) to U(IV) and subsequent UO_2
537 deposition because both brines were U-bearing and were therefore oxidized.

538 The new data from this study, in combination with the previously published data (Table 2),
539 together suggest that the basal sandstones of the Athabasca Group as well as the upper part of the
540 Athabasca Basement can be considered as a giant brine aquifer, at least at the scale of the present-
541 day Athabasca Basin. Knowledge of the vertical extent of brine circulation in the basement is
542 hindered by the lack of deep drill holes. The deepest known UO_2 mineralization in the basement
543 (400 m below the unconformity at Eagle Point) indicates a minimal depth for brine percolation. The
544 present-day maximum thickness of the basin is 1.5 km at Rumpel Lake. Assuming a past thickness
545 of around 3 to 6 km and a relatively flat-lying basement, the past extent of the basin could have
546 been much greater. As some deposits described in this study are located close to the basin margins
547 (Rabbit Lake) and even outside of the basin margins (Eagle Point), it can be inferred that the
548 circulation of the NaCl-rich and $CaCl_2$-rich brines extended beyond the present-day limits of the
549 basin, and that unconformity-related deposits are likely to have formed away from the present-day
550 limits. Interestingly, Mercadier et al. (2013) described alteration features typical of unconformity-
551 related U deposits around 20 km east of the present-day Athabasca Basin margins.
552
553

554 Origin and behavior of major solutes and metals

555

556 Many factors control the salinity and chemistry of basinal brines, including the composition of
557 seawater, evaporation of seawater, evaporite dissolution, dilution by meteoric water and/or
558 seawater, mixing of waters with different chemistry, and mineral buffering (Hanor 1994; Davisson
559 and Criss 1996; Houston et al. 2011). A common origin for the NaCl-rich and $CaCl_2$-rich brine end-
560 members identified in this study has been demonstrated from analysis of halogen (Cl–Br–I) and
561 noble gas (Ar–Kr–Xe) systematics and stable chlorine isotopic compositions of fluid inclusions
562 (Derome et al. 2005; Richard et al. 2011, 2014; Leisen et al. 2012). The halogen data show that the
563 two brines originated from a "parent brine" resulting from evaporation of seawater up to epsomite
564 saturation, leading to their high salinity. The composition of seawater at the time of sedimentation
565 in the Athabasca Basin remains unknown. The chemistry of evaporated seawaters is strongly
566 dependent on the initial seawater composition, which is thought to have oscillated throughout the
567 Phanerozoic and Neoproterozoic, between modern-like "$MgSO_4$ seas" and Cretaceous-like "$CaCl_2$
568 seas" (Lowenstein et al. 2001; Kovalevych et al. 2006). Whether the composition of seawater was
569 modern- or Cretaceous-like during sedimentation in the Athabasca Basin is unknown and both
570 hypotheses will be considered here. Evaporated seawater derived from "$CaCl_2$ seas" is considerably
571 more Ca-rich (although Na-dominated) than that derived from "$MgSO_4$ seas" (Lowenstein et al.
572 2001; Lowenstein and Timofeeff 2008). The compositions of the NaCl-rich and $CaCl_2$-rich brine
573 end-members do not plot between the epsomite-saturated evaporated seawater compositions for
574 "$MgSO_4$ seas" and "$CaCl_2$ seas", which may represent two extremes (Fig. 7). Regardless of the
575 seawater chemistry, it is clear that both NaCl-rich and $CaCl_2$-rich brines have compositions distinct
576 from that of their "parent brine". Therefore, it appears that the compositions of the two brines are
577 controlled not only by seawater evaporation, but also by different types of fluid-rock or fluid-fluid
578 interactions. As the salinity of the NaCl and $CaCl_2$-rich brines is close to that of epsomite-saturated

evaporated seawater, it is assumed that most of the reactions that significantly contributed to the modification of the composition of the initial evaporated seawater are ion exchange reactions or mixing between brines of comparable salinity. In Figure 7, the directions of compositional shifts expected for some typical fluid-rock or fluid-fluid interactions have been plotted. The interactions considered are: (1) halite dissolution or mixing with halite-dissolution fluid, which leads to Na-dominated compositions; (2) dolomitization of calcite (1:1 Mg/Ca exchange); (3) albitization of plagioclase (2:1 Na/Ca exchange); (iv) albitization of K-feldspar (1:1 Na/K exchange) and (5) Mg-alteration typical of unconformity-related U deposits (replacement of initial silicates, except quartz, by sudoite and dravite). Mg alteration is broadly characterized by Mg input and Ca-Na-K loss in the altered rocks. The precise chemical budget of Mg-alteration is difficult to constrain, the relative and absolute amounts of Ca, Na and K lost being dependent on the lithology and degree of alteration (Alexandre et al. 2005). In Figure 7, Mg-alteration is represented as net Mg-loss in the fluid. If the composition of the parent brine was that of "$MgSO_4$ seas" evaporated-seawater, then the composition of the NaCl-rich brine is best explained by a combination of halite dissolution or mixing with halite-dissolution fluid, Mg-alteration, dolomitization and albitization. In the same scenario, the composition of the $CaCl_2$-rich brine is best explained by a combination of albitization and dolomitization. If the composition of the parent brine is that of a "$CaCl_2$ seas" evaporated-seawater, then the composition of the NaCl-rich brine is best explained by halite dissolution or mixing with halite-dissolution fluid alone. In the same scenario, the composition of the $CaCl_2$-rich brine can be explained by albitization alone. Dolomitization and mixing with halite-dissolution brine (or halite dissolution) can occur at shallow depths, close to the depositional environment. Note that mixing with halite-dissolution brine is preferred to halite dissolution because the investigated brines are highly saline and would probably not have been able to dissolve halite. Albitization could have occurred at greater depth in the basin (in the eroded part because no detrital K-feldspars/plagioclase are currently present) or in the basement. Petrographic evidence for

albitization due to basinal brines in the basement is lacking. However, sampling has been limited to relatively shallow drillcores and albitization at depth in the basement cannot be ruled out. The influence of Mg-alteration is difficult to ascertain. Though Mg-alteration could explain part of the variability in the Mg concentration of the $CaCl_2$-rich brine end-member and part of the Mg-depleted composition of the NaCl-rich brine end-member, it is not the dominant control on the brine chemistry. Taken together, the fluid inclusion data are most simply explained by considering a "$CaCl_2$ seas" evaporated-seawater parent brine. In order to form the $CaCl_2$-rich brine, the parent brine may have escaped dolomitization and mixing with halite-dissolution brine, probably by migrating from the evaporitic environment (laterally and/or vertically) shortly after the evaporative process, and then undergone albitization. In order to form the NaCl-rich brine, the parent brine is more likely to have remained spatially connected to the evaporitic environment and was more susceptible to modification by halite dissolution and/or mixing with halite-dissolution brine and dolomitization (Warren 1997; Houston et al. 2011). It is clear that these assumptions are only a first-order approach to the fluid-rock interactions that could have occurred in the Athabasca Basin. For example, the importance of mixing with halite-dissolution brines has probably been overestimated because the large contribution of halite-dissolution brine to the composition of the NaCl-rich brine cannot account for the observed Cl/Br ratios and $\delta^{37}Cl$ values of fluid inclusions (Richard et al. 2011; 2014; Leisen et al. 2012). Moreover, estimating the contributions of each of the reactions invoked is complicated by the number of reactions considered and the uncertainties in the compositions of parent brines and brine end-members. Nevertheless, the two brines may have had very distinct interaction histories and consequently, distinct pathways.

Metal-rich basinal brines are commonly sampled from boreholes or fluid inclusions and the connection between basinal brines and basin-hosted mineral deposits has been established in several studies (Carpenter et al. 1974; Sverjensky 1984, 1989; Kharaka et al. 1987; Kharaka and Hanor 2003; Wilkinson et al. 2009; Richard et al. 2012). The metal concentrations in the Athabasca brines

629 can be compared with those of present-day sedimentary formation brines and those derived from
630 LA-ICP-MS analysis of fluid inclusions from various basin-hosted base-metal ore deposits
631 worldwide (Fig. 10). This comparison is limited by the limits of detection for metals by LA-ICP-
632 MS which precludes the determination of metals with concentrations below 0.1 ppm. The
633 Athabasca brines have Ba, Mn, Zn and Pb concentrations comparable to the highest concentrations
634 recorded in sedimentary formation brines, whereas Fe, Cu and, more spectacularly, U
635 concentrations are clearly above the richest Fe, Cu and U-bearing sedimentary formation brines
636 (Carpenter et al. 1974; Kraemer and Kharaka 1986; Kharaka et al. 1987; Banner et al. 1990;
637 Connolly et al. 1990; Stueber and Walter 1991; Land and Macpherson 1992; Pluta and Zuber 1995;
638 Hodge et al. 1996; Hitchon et al. 2001; Aquilina et al. 2002). The Athabasca brines have Fe, Ba,
639 Mn, Cu, Zn, Pb concentrations that are comparable to the highest concentrations recorded by LA-
640 ICP-MS analysis of fluid inclusions in basin-hosted base metal ore fluids (Appold et al. 2004;
641 Stoffell et al. 2004; Bouch et al. 2006; Huizenga et al. 2006; Piqué et al. 2008; Stoffell et al. 2008;
642 Sanchez et al. 2009; Wilkinson et al. 2009; Appold and Wenz, 2011). No data is available for U
643 concentrations in basin-hosted base metal ore fluids. The U concentrations in the Athabasca brines
644 are among the most elevated concentrations recorded for geological fluids so far and are discussed
645 in detail in Richard et al. (2012). However, other U deposits also show ore-forming brines with U
646 concentrations of tens of ppm (Eglinger et al. 2014; Hurtig et al. 2014) meaning this could be a
647 more general characteristic of U ore-forming fluids. Basinal brines can be driven through basement
648 rocks in response to basement fracturing, resulting in intense fluid-rock interaction and metal
649 extraction, and ultimately in the formation of Pb, Zn, Cu, F, Ba and U deposits close to the
650 basement-cover interface (e.g. Shelton et al. 1995; Gleeson et al. 2000; Boiron et al. 2002, 2010;
651 Feltrin et al. 2003; Kendrick et al. 2005; Wilkinson et al. 2005; Muchez et al. 2005; McGowan et al.
652 2006; Oliver et al. 2006; Kozyi et al. 2009; Mercadier et al. 2010; Cathelineau et al. 2012;
653 Fusswinkel et al. 2014). Petrological and geochemical evidence for U mobilization from the

654 Athabasca Basement sources (e.g. monazite, pre-Athabasca Basin UO_2) is widespread (Annesley
655 and Madore 1999; Hecht and Cuney 2000; Cuney et al. 2010; Mercadier et al. 2013). If, as
656 indicated by the contrasting metal loads of the two brine end-members (Fig. 8), the $CaCl_2$-rich brine
657 acquired more metals than the NaCl-rich brine and if the basement is effectively the main U source,
658 then it could well be that the $CaCl_2$-rich brine leached metals from the basement more efficiently
659 than the NaCl-rich brine.

660 Hacini and Oelkers (2011) have shown that U can be conservative during evaporative
661 processes. This means that no U-bearing phase precipitates and the U is not substituted by any other
662 elements in the evaporitic minerals during evaporation. Li is another conservative element during
663 evaporation. Therefore, Li/U ratios should remain constant during seawater evaporation. Assuming
664 Li and U concentrations in seawater of 170 and 3.3 ppb, respectively (Ku et al. 1977; Drever 1982)
665 and a Li concentration in epsomite-saturated evaporated seawater of ~10 ppm (Fontes and Matray
666 1993), the U concentration in epsomite-saturated evaporated seawater should be close to 0.2 ppm.
667 This corresponds to the lowest U concentration measured during LA-ICP-MS analysis of fluid
668 inclusions. Hence, it is possible that evaporation of seawater was the first U-enrichment process to
669 occur in the studied brines, although further strong enrichment is required to account for the high U
670 concentrations in the fluid inclusions. Given the solubility of U(VI) in such brines, and the U
671 concentrations measured in the fluid inclusions, the pH of the NaCl and $CaCl_2$-rich brines may have
672 been between 2.5 and 4.5 (Richard et al. 2012). The acidic nature of the brines may also have
673 promoted the transport of Ba, Mn, Cu, Pb, and Zn. The redox processes at the origin of UO_2
674 deposition are still poorly understood (Hoeve and Quirt 1987; Richard et al. 2013a) and will not be
675 discussed here, but they were probably active only at the ore deposit sites as similar NaCl- and
676 $CaCl_2$-rich brines were present not only in mineralized but also in unmineralized areas such as
677 Rumpel Lake (Table 2). Although the Athabasca brines have metal concentrations comparable to
678 those of a number of world-class basin-hosted base metal deposits (Fig. 10), the absence of

679 deposition of Pb, Zn, Ba or Cu-bearing sulphide phases is intriguing. Minor sulphide and arsenide
680 minerals containing Fe, Ni, Co, Cu, Pb, Zn, As, Mo and occasionally Au, Ag, Se and platinum
681 group elements, have been identified around the studied deposits (Ruzicka 1989). However, the
682 precise paragenetic position of these minerals with respect to U deposition remains unclear. The
683 only significant S-bearing alteration minerals found here are the aluminium phosphate-sulphate
684 minerals (Gaboreau et al. 2007). In general, causes for deposition of base metal sulphides in basinal
685 settings are (i) reduction of sulfate to reduced sulfur by thermochemical sulfate reduction (TSR) or
686 bacterial sulfate reduction (BSR) (Machel 2001); and (ii) mixing between metal-bearing fluids with
687 cooler and/or dilute fluids which favors destabilization of metal complexes or with H_2S-bearing
688 fluids. The Athabasca brines contain negligible sulfates (Richard et al. 2011) and Raman
689 investigation of fluid inclusions revealed an absence of H_2S (Derome et al. 2003). Furthermore, the
690 Athabasca brines did not mix with low-salinity-fluids. Therefore, the conditions for base metal
691 deposition were not met in the Athabasca system.
692
693 **Conclusion**
694
695 Microthermometry and LA-ICP-MS analysis of fluid inclusions from five unconformity-related U
696 deposits in the Athabasca Basin and Basement (Canada) allows to define the general characteristics
697 of the metal-rich brines that were the dominant fluids involved before, during and after UO_2
698 deposition:
699 (1) NaCl-rich and $CaCl_2$-rich brines previously described at the McArthur River deposit have
700 been reported for all of the newly studied deposits (Rabbit Lake, P-Patch, Eagle Point, Shea
701 Creek and Millennium). A reappraisal of previously published fluid inclusion data suggest
702 that these brines were also present in all previously studied deposits (Midwest, Cluff Lake,

703 Sue C - McClean, Key Lake), and also in unmineralized central parts of the basin (Rumpel
704 Lake). Brine circulation was therefore probably basin-scale.
705 (2) The NaCl-rich brine (T-P: 180 ± 30°C and 800 ± 400 bars) and the $CaCl_2$-rich brine (T-P:
706 120 ± 30°C and 600 ± 300 bars) have mixed in all deposits, under pressure conditions that
707 have probably fluctuated between hydrostatic and supra-hydrostatic. However, the two
708 brines show U contents indicative of relatively high oxygen fugacity. Therefore, brine
709 mixing was probably not the driving force for uranium reduction and precipitation.
710 (3) The two brines were chemically differentiated from their common parent composition
711 (epsomite-saturated evaporated seawater) along distinct flow paths and fluid-rock
712 interaction. The NaCl-rich brine underwent a possible combination of Mg/Ca exchange by
713 dolomitization, mixing with halite-dissolution brine and Na/Ca and/or Na/K exchange by
714 albitization. The $CaCl_2$-rich brine underwent nearly complete Na/Ca and/or Na/K exchange
715 possibly by albitization.
716 (4) The two brines have high metal contents, the $CaCl_2$-rich brine being up to one order of
717 magnitude more enriched in Cu, Pb, Zn, Mn and U. The metal concentrations are higher
718 than in high-salinity sedimentary formation waters worldwide and are comparable to those
719 found in fluid inclusions from basin-hosted Pb-Zn deposits, for which a basement metal
720 source has been frequently invoked.
721 Finally, this study shows that the most spectacular uranium province in the world resulted from
722 large-scale circulation of surface-derived brines (evaporated seawater), over hundreds of kilometres
723 laterally, across an entire 3-6 km-thick sedimentary pile and at least several hundreds of meters
724 below the unconformity in the crystalline basement. Such a large-scale brine circulation may have
725 been a key parameter for the mobilization of huge amounts of uranium and other metals in the
726 mineralizing systems.
727

Acknowledgements

The authors thank CNRS and Areva NC for the financial support (BDI CNRS-Areva NC PhD grant for A. Richard and J. Mercadier); Donatienne Derome for early microthermometric work; Areva NC and Cameco for providing the samples and Cédric Demeurie for preparation of doublypolished thick sections. The authors greatly appreciated insightful comments by Guoxiang Chi on an earlier version of this paper. The comments of two anonymous reviewers as well as the editorial suggestions from Rolf Romer and Georges Beaudoin helped to greatly improve the manuscript.

References

Alexandre P, Kyser K, Polito P, Thomas D (2005) Alteration mineralogy and stable isotope geochemistry of Paleoproterozoic basement-hosted unconformity-type uranium deposits in the Athabasca Basin, Canada. Econ Geol 100:1547–1563

Alexandre P, Kyser K, Thomas D, Polito P, Marlat J (2009) Geochronology of unconformity-related uranium deposits in the Athabasca Basin, Saskatchewan, Canada and their integration in the evolution of the basin. Miner Deposita 44:41–59

Alexandre P. Kyser K, Jiricka D, Witt G (2012) Formation and evolution of the Centennial unconformity-related uranium deposit in the South-Central Athabasca Basin, Canada. Econ Geol 107:385–400

Allan MM, Yardley BWD, Forbes LJ, Shmulovich KI, Banks DA, Shepherd TJ (2005) Validation of LA-ICP-MS fluid inclusion analysis with synthetic fluid inclusions. Am Mineral 90:1767–1775

751 Annesley IR, Madore C (1999) Leucogranites and pegmatites of the sub-Athabasca basement,
752 Saskatchewan: U protore? In: Stanley CJ et al. (eds.), Mineral Deposits: Processes to
753 Processing. Balkema, Rotterdam, pp 297–300
754 Annesley IR, Madore C, Portella P (2005) Geology and thermotectonic evolution of the western
755 margin of the Trans-Hudson Orogen: Evidence from the eastern sub-Athabasca basement,
756 Saskatchewan. Can J Earth Sci 42:573–597
757 Appold MS, Numelin TJ, Shepherd TJ, Chenery SR (2004) Limits on the metal content of fluid
758 inclusions in gangue minerals from the Viburnum Trend, Southeast Missouri, determined by
759 laser ablation ICP-MS. Econ Geol 99:185–198
760 Appold MS, Wenz ZJ (2011) Composition of ore fluid inclusions from the Viburnum Trend,
761 Southeast Missouri district, United States: Implications for transport and precipitation
762 mechanisms. Econ Geol 106:55–78
763 Aquilina L, Ladouche B, Doerfliger N, Seidel JL, Bakalowicz M, Dupuy C, Le Strat P (2002)
764 Origin, evolution and residence time of saline thermal fluids (Balaruc springs, southern
765 France): implications for fluid transfer across the continental shelf. Chem Geol 192:1–21
766 Bakker RL (2003) Package FLUIDS 1. Computer programs for analysis of fluid inclusion data and
767 for modelling bulk fluid properties. Chem Geol 194:3–23
768 Banner JL, Wasserburg GJ, Chen JH, Moore CH (1990) ^{234}U-^{238}U-^{230}Th-^{232}Th systematics in saline
769 groundwaters from central Missouri. Earth Planet Sci Lett 101:296–312
770 Becker SP, Fall A, Bodnar RJ (2008) Synthetic fluid inclusions XVII. PVTX properties of high
771 salinity H_2O-NaCl solutions (>30 wt % NaCl): Application to fluid inclusions that
772 homogenize by halite disappearance from porphyry copper and other hydrothermal ore
773 deposits. Econ Geol 103:539–554

774 Behr HJ, Horn EE, Frentzel-Beyme K, Reutel C (1987) Fluid inclusion characteristics of the
775 Variscan and post-Variscan mineralizing fluids in the Federal Republic of Germany. Chem
776 Geol 61: 273–285
777 Beshears CJ (2010) The geology and geochemistry of the Millennium deposit, Athabasca Basin,
778 Saskatchewan, Canada. Unpub. MSc thesis, University of Manitoba, 133 p
779 Boiron MC, Cathelineau M. Banks DA, Buschaert S, Fourcade S, Coulibaly Y, Michelot JL, Boyce
780 A (2002) Fluid transfers at a basement/cover interface: Part II. Large-scale introduction of
781 chlorine into the basement by Mesozoic basinal brines. Chem Geol 192:121–140
782 Boiron MC, Cathelineau M, Richard A (2010) Fluid flows and metal deposition near
783 basement/cover unconformity: lessons and analogies from Pb–Zn–F–Ba systems for the
784 understanding of Proterozoic U deposits. Geofluids 10:270–292
785 Bons PD, Fusswinkel T, Gomez-Rivas E, Markl G, Wagner T, Walter B (2014) Fluid mixing from
786 below in unconformity-related ore deposits. Geology 42: 1035–1038
787 Bodnar RJ (2003) Reequilibration of fluid inclusions. In: Samson I, Anderson A, Marshall D.
788 (eds.), Fluid Inclusions: Analysis and Interpretation. Mineralogical Association of Canada
789 Short Course Series 32, pp. 213–230
790 Bouch J.E. Naden J. Shepherd TJ, McKervey JA, Young B, Benham AJ, Sloane HJ (2006) Direct
791 evidence of fluid mixing in the formation of stratabound Pb–Zn–Ba–F mineralisation in the
792 Alston Block, North Pennine Orefield (England). Miner Deposita 41:821–835
793 Card, C., Portella, P., Annesley, I., Pana, D., 2007. Basement rocks to the Athabasca basin.
794 Geological Survey of Canada Bulletin 588, pp. 69–87
795 Carpenter A.B, Trout ML, Pickett EE (1974) Preliminary report on the origin and chemical
796 evolution of lead- and zinc-rich brines in central Mississippi. Econ Geol 69:1191–1206
797 Cathelineau M, Boiron MC, Fourcade S, Ruffet G, Clauer N, Belcourt O, Coulibaly Y, Banks DA,
798 Guillocheau F (2012) A major Late Jurassic fluid event at the basin/basement unconformity

799 in western France: $^{40}Ar/^{39}Ar$ and K–Ar dating, fluid chemistry, and related geodynamic
800 context. Chem Geol 322–323:99–120
801 Chi G, Bosman S, Card C (2013) Numerical modeling of fluid pressure regime in the Athabasca
802 basin and implications for fluid flow models related to the unconformity-type uranium
803 mineralization. J Geochem Explor 125:8–19
804 Chiarenzelli J, Aspler L, Villeneuve M, Lewry J (1998) Early Proterozoic evolution of the
805 Saskatchewan craton and its allochtonous cover, Trans-Hudson orogen. J Geol 106:247–267
806 Cloutier J, Kyser K, Olivo GR, Alexandre P, Halaburda J (2009) The Millennium uranium deposit,
807 Athabasca Basin, Saskatchewan, Canada: An atypical basement-hosted unconformity-
808 related uranium deposit. Econ Geol 104: 815–840
809 Cloutier, J., Kyser, K., Olivo, G., Brisbin, D., 2011. Geochemical, isotopic, and geochronologic
810 constraints on the formation of the Eagle Point basement-hosted uranium deposit, Athabasca
811 Basin, Saskatchewan, Canada and recent remobilization of primary uraninite in secondary
812 structures. Miner Deposita 46, 35–56
813 Connolly CA, Walter LM, Baadsgaard H, Longstaffe F (1990) Origin and evolution of formation
814 waters, Alberta Basin, Western Canada Sedimentary Basin. 1. Isotope systematics and water
815 mixing. Appl Geochem 5:397–413
816 Cui T, Yang J, Samson I, (2012a). Tectonic deformation and fluid flow: Implications for the
817 formation of unconformity-related uranium deposits. Econ Geol 107:147–163
818 Cui T, Yang J, Samson I (2012b) Solute transport across basement/cover interfaces by buoyancy
819 driven thermohaline convection: Implications for the formation of unconformity-related
820 uranium deposits. Am J Sci 312:994–1027
821 Cumming GL, Krstic D (1992) The age of unconformity-related uranium mineralization in the
822 Athabasca Basin, northern Saskatchewan. Can J Earth Sci 29:1623–1639

823 Cuney M (2010) Evolution of uranium fractionation processes through time: Driving the secular
824 variation of uranium deposit types. Econ Geol 105:553–569
825 Dahlkamp FJ (1978) Geologic appraisal of the Key Lake U-Ni deposits, northern Saskatchewan:
826 Econ Geol 73:1430–1449
827 Dargent M, Dubessy J, Truche L, Bazarkina EF, Nguyen-Trung C, Robert P (2013) Experimental
828 study of uranyl(VI) chloride complex formation in acidic LiCl aqueous solutions under
829 hydrothermal conditions (T = 21°C–350°C, Psat) using Raman spectroscopy. Eur J Mineral
830 25:765–775
831 Davisson ML, Criss RE (1996) Na-Ca-Cl relations in basinal fluids. Geochim Cosmochim Acta
832 60:2743–2752
833 Derome D, Cathelineau M, Lhomme T, Cuney M (2003) Fluid inclusion evidence of the differential
834 migration of H_2 and O_2 in the McArthur River unconformity-type uranium deposit
835 (Saskatchewan, Canada). Possible role on post-ore modifications of the host rocks. J
836 Geochem Explor 78–79:525–530
837 Derome D, Cathelineau M, Cuney M, Fabre C, Lhomme T, Banks DA (2005) Mixing of sodic and
838 calcic brines and uranium deposition at the McArthur River, Saskatchewan, Canada. A
839 Raman and laser-induced breakdown spectroscopic study of fluid inclusions. Econ Geol
840 100:1529–1545
841 Drever JI (1982) The Geochemistry of Natural Waters. Prentice Hall, Englewood Cliffs, N.J., 338 p
842 Dubessy J, Derome D, Sausse J (2003) Numerical modelling of fluid mixings in the H_2O-NaCl
843 system. Applications to the North Caramal uranium prospect (Australia). Chem Geol
844 194:25–39
845 Earle S, Sopuck V (1989) Regional lithogeochemistry of the eastern part of the Athabasca Basin
846 uranium province, Saskatchewan. In: Muller-Kahle E (ed), Uranium Resources and Geology
847 of North America. International Agency of Nuclear Energy TECHDOC-500, pp. 263–269

848 Eglinger A, Ferraina C, Tarantola A, André-Mayer AS, Vanderhaeghe O, Boiron MC, Dubessy J,
849 Richard A, Brouand M (2014) Hypersaline fluids generated by high-grade metamorphism of
850 evaporites: fluid inclusion study of uranium occurrences in the Western Zambian
851 Copperbelt. Contrib Mineral Petr 167 in press, doi: 10.1007/s00410-014-0967-9
852 Essarraj S, Boiron MC, Cathelineau M, Banks DA, Benharref M (2005) Penetration of surface-
853 evaporated brines into the Proterozoic basement and deposition of Co and Ag at Bou Azzer
854 (Morocco): Evidence from fluid inclusions. J Afr Earth Sci 41:25–39
855 Fayek M. Kyser TK (1997) Characterization of multiple fluid-flow events and rare-earth-element
856 mobility associated with formation of unconformity-type uranium deposits in the Athabasca
857 Basin, Saskatchewan. Can Mineral 35:627–658
858 Feltrin L, Oliver NHS, Kelso IJ, King S (2003) Basement metal scavenging during basin evolution:
859 Cambrian and Proterozoic interaction at the Century Zn-Pb-Ag Deposit, Northern Australia.
860 J Geochem Explor 78–79:159–162
861 Fontes JC, Matray JM (1993) Geochemistry and origin of formation brines from the Paris Basin,
862 France 1. Brines associated with Triassic salts. Chem Geol 109:149–175
863 Freiberger R, Cuney M (2003) New evidence for extensive fluid-circulations within the basement in
864 relation to unconformity type uranium deposit genesis in the Athabasca basin,
865 Saskatchewan, Canada. Proceedings of International Conference Uranium Geochemistry
866 2003, Nancy, pp. 151–154
867 Fusswinkel T, Wagner T, Wälle M, Wenzel T, Heinrich CA, Markl G (2013) Fluid mixing forms
868 basement-hosted Pb-Zn deposits: Insight from metal and halogen geochemistry of individual
869 fluid inclusions. Geology 41, 679–682
870 Gaboreau S, Cuney M, Quirt D, Beaufort D, Patrier P, Mathieu R (2007) Significance of aluminium
871 phosphate-sulfate minerals associated with U unconformity-type deposits: the Athabasca
872 basin, Canada. Am Mineral 92:267–280

873 Genest S, Robert F, Duhamel I (2010) The Carswell impact event, Saskatchewan, Canada:
874 Evidence for a pre-Athabasca multiring basin? Geol Society Am S 465:543–570
875 Gleeson S, Yardley BWD, Boyce AJ, Fallick AE, Munz IA (2000) From basin to basement: the
876 movement of surface fluids into the crust. J Geochem Explor 69–70:527–531
877 Gleeson SA, Yardley BWD, Munz IA, Boyce AJ (2003) Infiltration of basinal fluids into high-
878 grade basement, South Norway: sources and behaviour of waters and brines. Geofluids
879 3:33–48
880 Goldstein RH, Reynolds TJ (1994) Systematics of fluid inclusions in diagenetic minerals. Society
881 of Economic Paleontologists and Mineralogists (SEPM) Short Course Volume 31, 198 p
882 Goldstein RH (2001) Fluid inclusions in sedimentary and diagenetic systems. Lithos 55:159–193
883 Guillong M, Meier DL, Allan M, Heinrich CA, Yardley BWD (2008) SILLS: A Matlab-based
884 program for the reduction of laser ablation ICP-MS data of homogeneous materials and
885 inclusions. In: Sylvester P (ed.), Laser Ablation ICP–MS in the Earth Sciences: Current
886 Practices and Outstanding Issues. Mineralogical Association of Canada Short Course Series
887 40, pp. 328–333
888 Hacini M Oelkers EH (2011) Geochemistry and behavior of trace elements during the complete
889 evaporation of the Merouane Chott ephemeral lake: Southeast Algeria. Aquat Geochem
890 17:51–70
891 Hanor JS (1994) Origin of saline fluids in sedimentary basins. In: Parnell J (ed.), Geofluids: Origin,
892 Migration and Evolution of Fluids in Sedimentary Basins. Geol Soc SP 78:151–174
893 Haynes FM (1985) Determination of fluid inclusion compositions by sequential freezing. Econ
894 Geol 80:1436–1439
895 Hecht L, Cuney M (2000) Hydrothermal alteration of monazite in the Precambrian crystalline
896 basement of the Athabasca Basin (Saskatchewan, Canada): Implications for the formation of
897 unconformity-related uranium deposits. Miner Deposita 35:791–795

898 Heine TH (1986) The geology of the Rabbit Lake uranium deposit, Saskatchewan. In: Evans EL
899 (ed.), Uranium deposits of Canada. Canadian institute of Mining, Metallurgy and Petroleum
900 Special Volume 33, pp. 134–143
901 Hitchon B, Perkins EH, Gunter WD (2001) Recovery of trace metals in formation waters using acid
902 gases from natural gas. Appl Geochem 16:1481–1497
903 Hodge VF, Johannesson KH, Stetzenbach KJ (1996) Rhenium, molybdenum, and uranium in
904 groundwater from the southern Great Basin, USA. Geochim Cosmochim Acta 60:3197–
905 3214
906 Hoeve J, Sibbald TII (1978) On the genesis of the Rabbit Lake and other unconformity-type
907 uranium deposits in Northern Saskatchewan, Canada. Econ Geol 73:1450–1473
908 Hoeve J, Kyser TK, Forester RW (1986) Cover-basement interaction and the origin of U-Ni-Co
909 mineralization in the Athabsca Basin: Isotopic evidence (O, H, C). Saskatchewan Research
910 Council Publication No. R-855-3-A-86. 89 pp
911 Hoeve J, Quirt DA (1987) A stationary redox front as a critical factor in the formation of high-
912 grade, unconformity-type uranium ores in the Athabasca Basin, Saskatchewan, Canada. B
913 Mineral 110:151–171
914 Hoffman P (1990) Subdivision of the Churchill Province and extent of the Trans-Hudson Orogen.
915 In: Lewry JF, Stauffer MR (eds.), The Early Proterozoic Trans-Hudson Orogen of North
916 America. Geological Association of Canada Special Paper 37:15–39
917 Houston S, Smalley C, Laycock A, Yardley BWD (2011) The relative importance of buffering and
918 brine inputs in controlling the abundance of Na and Ca in sedimentary formation waters.
919 Mar Petrol Geol 28:1242–1251
920 Huizenga JM, Gutzmer J, Banks DA, Greyling L (2006) The Palaeoproterozoic carbonate-hosted
921 Pering Pb-Zn deposit, South Africa. 2: fluid inclusion, fluid chemistry and stable isotope
922 constrains. Miner Deposita 40, 686–706

923 Hurtig NC, Heinrich CA, Driesner T, Herrmann W, Wall V, Mathison I (2014) Fluid evolution and
924 uranium (-Mo-F) mineralization at the Maureen Deposit (Queensland, Australia):
925 Unconformity-related hydrothermal ore formation with a source in the volcanic cover
926 Sequence. Econ Geol 109: 737–773
927 Jefferson CW, Thomas DJ, Gandhi SS, Ramaekers P, Delaney G, Brisbin D, Cutts C, Portella P,
928 Olson RA (2007). Unconformity associated uranium deposits of the Athabasca Basin,
929 Saskatchewan and Alberta. Geological Survey of Canada Bulletin 588:23–67
930 Kendrick MA, Burgess R, Harrison D, Bjorlykke A (2005) Noble gas and halogen evidence for the
931 origin of Scandinavian sandstone-hosted Pb-Zn deposits. Geochim Cosmochim Acta
932 69:109–129
933 Kharaka YK, Maest AS, Carothers WW, Law LM, Lamothe PJ, Fries TL (1987) Geochemistry of
934 metal-rich brines from central Mississippi Salt Dome basin, U.S.A. Appl Geochem 2:543–
935 561
936 Kharaka YK, Hanor JS (2003) Deep Fluids in the Continents: I. Sedimentary Basins. In: Holland
937 HD, Turekian KK (eds.), Treatise on Geochemistry, Volume 5. Elsevier, pp. 499–540
938 Kister P, Laverret E, Quirt D, Cuney M, Patrier P, Beaufort D, Bruneton P (2006) Mineralogy and
939 geochemistry of the host-rock alterations associated to the Shea Creek unconformity-type
940 uranium deposits (Saskatchewan, Canada), Part 2. Spatial distribution of the Athabasca
941 Group sandstone matrix minerals. Clay Clay Miner 54:295–313
942 Kraemer TF, Kharaka YK (1986) Uranium geochemistry in geopressured-geothermal aquifers of
943 the U.S. Gulf Coast. Geochim Cosmochim Acta 50:1233–1238
944 Kovalevych VM, Marshall T, Peryt TM, Petrychenko OY, Zhukova SA (2006) Chemical
945 composition of seawater in Neoproterozoic: Results of fluid inclusion study of halite from
946 Salt Range (Pakistan) and Amadeus Basin (Australia). Precambrian Res 144:39–51

947 Kotzer TG, Kyser TK, Irving E (1992) Paleomagnetism and the evolution of fluids in the
948 Proterozoic Athabasca Basin, Northern Saskatchewan, Canada. Can J Earth Sci 29:1474–
949 1491
950 Kotzer TG, Kyser TK (1995) Petrogenesis of the Proterozoic Athabasca Basin, Northern
951 Saskatchewan, Canada, and its relation to diagenesis, hydrothemal uranium mineralization
952 and paleohydrogeology. Chem Geol 120:45–89
953 Koziy L, Bull S, Large R, Selley D (2009) Salt as a fluid driver, and basement as a metal source, for
954 stratiform sediment-hosted copper deposits. Geology 37:1107–1110
955 Ku, TL, Knauss KG, Mathieu GG (1977) Uranium in open ocean: concentration and isotopic
956 composition. Deep Sea Research 24:1005–1117.
957 Kyser TK, Hiatt E, Renac C, Durocher K, Holk G, Deckart K (2000) Diagenetic fluids in paleo- and
958 meso-proterozoic sedimentary basins and their implications for long protracted fluid
959 histories. In: Kyser K. (ed.), Fluids and basin evolution. Mineralogical association of
960 Canada Short Course Series 28, pp. 225–262
961 Kyser TK, Cuney M (2008) Unconformity-related uranium deposits. In: Cuney M, Kyser K (eds.),
962 Recent and Not-So-Recent Developments in Uranium Deposits and Implications for
963 Exploration. Mineralogical Association of Canada Short Course Series 39, pp. 161–219
964 Land LS, Macpherson GL (1992) Origin of saline formation waters, Cenozoic section, Gulf of
965 Mexico sedimentary basin. Am Assoc Petr Geol B 76:1344–1362
966 Lawler JP, Crawford ML (1982) Fluid inclusions in the Midwest Lake Uranium deposit. Geological
967 Society of America, Abstracts with Programs 14, pp. 542
968 Leisen M, Boiron MC, Richard A, Dubessy J (2012) Determination of Cl and Br concentrations in
969 individual fluid inclusions by combining microthermometry and LA-ICPMS analysis:
970 Implications for the origin of salinity in crustal fluids. Chem Geol, 330–331:197–206

971 Lorilleux G, Jébrak M, Cuney M, Baudemont D (2002) Polyphase hydrothermal breccia associated
972 with unconformity-related uranium mineralizations (Canada). From fractal analysis to
973 structural significance. J Struct Geol 24:323–338
974 Lorilleux G, Cuney M, Jébrak M, Rippert JC, Portella P (2003) Chemical brecciation processes in
975 the Sue unconformity-type uranium deposits, Eastern Athabasca Basin (Canada). J Geochem
976 Explor 80:241–258
977 Longerich HP, Jackson SE, Günther D (1996) Laser ablation inductively coupled plasma mass
978 spectrometric transient signal data acquisition and analyte concentration calculation. J Anal
979 Atom Spectrom 11:899–904
980 Lowenstein TK, Timofeeff MN, Brennan ST, Hardie LA, Demicco RV (2001) Oscillations in
981 Phanerozoic seawater chemistry: Evidence from fluid inclusions. Science 294:1086–1088
982 Lowenstein TK, Timofeeff MN (2008) Secular variations in seawater chemistry as a control on the
983 chemistry of basinal brines: test of the hypothesis. Geofluids 8:77–92
984 McGowan RR, Roberts S, Boyce AJ (2006) Origin of the Nchanga copper-cobalt deposits of the
985 Zambian Copperbelt. Miner Deposita 40:617–638
986 Mercadier J, Richard A, Boiron MC, Cathelineau M, Cuney M (2010) Brine migration in the
987 basement rocks of the Athabasca Basin through microfracture networks (P-Patch U deposit,
988 Canada). Lithos 115:121–136
989 Mercadier J, Cuney M, Cathelineau M, Lacorde M (2011a) U redox fronts and kaolinisation in
990 basement-hosted unconformity-related U ores of the Athabasca Basin (Canada): late U
991 remobilisation by meteoric fluids. Miner Deposita 46:105–135
992 Mercadier J, Cuney M, Lach P, Boiron MC, Bonhoure J, Richard A, Leisen M, Kister P (2011b)
993 Origin of uranium deposits revealed by their rare earth element signature. Terra Nova
994 23:264–269

995 Mercadier J, Richard A, Cathelineau M (2012) Boron- and magnesium-rich marine brines at the
996 origin of giant unconformity-related uranium deposits: $\delta^{11}B$ evidence from Mg-tourmalines.
997 Geology 40:231–234
998 Mercadier J, Annesley IR, McKechnie CL, Bogdan TS, Creighton S (2013) Magmatic and
999 metamorphic uraninite mineralization in the western margin of the Trans-Hudson Orogen
1000 (Saskatchewan, Canada): a uranium source for unconformity-related uranium deposits?
1001 Econ Geol 108, 1037–1065
1002 Muchez P, Heijlen W, Banks DA, Blundell D, Boni M, Grandia F (2005) Extensional tectonics and
1003 the timing and formation of basin-hosted deposits in Europe. Ore Geol Rev 27:241–267
1004 Munz IA, Yardley BWD, Banks DA, Wayne DW (1995) Deep penetration of sedimentary fluids in
1005 basement rocks from southern Norway: Evidence from hydrocarbon and brine inclusions.
1006 Geochim Cosmochim Acta 59:239–254
1007 Ng R, Alexandre P, Kyser K (2013) Mineralogical and Geochemical Evolution of the
1008 Unconformity-Related McArthur River Zone 4 Orebody in the Athabasca Basin, Canada:
1009 Implications of a Silicified Zone. Econ Geol 108:1657–1689
1010 Oliver NHS, McLellan JG, Hobbs BE, Cleverly JS, Ord A, Feltrin L (2006) Numerical models of
1011 extensional deformation, heat transfer, and fluid flow across basement-cover interfaces
1012 during basin-related mineralization. Econ Geol 101:1–31
1013 Pagel M (1975a) Cadre Géologique des gisements d'uranium dans la structure Carswell
1014 (Saskatchewan – Canada) – « Etude des phases fluides ». Unpub. PhD thesis, Université de
1015 Nancy 1, 157 p
1016 Pagel M (1975b) Détermination des conditions physico-chimiques de la silicification diagénétique
1017 des grès Athabasca (Canada) au moyen des inclusions fluides. Comptes Rendus de
1018 l'Académie des Sciences de Paris 280:2301–2304

1019 Pagel M, Poty B, Sheppard SMF (1980) Contribution to some Saskatchewan uranium deposits
1020 mainly from fluid inclusion and isotopic data. In: IAEA (ed.), International Uranium
1021 Symposium on the Pine Creek Geosyncline, Vienna, pp. 639–654
1022 Pagel M, Wheatley K, Ey F (1985) Origin of the Carswell circular structure. A summary of data for
1023 geological interpretation of its formation. In: Laine R, Alonso D, Svab M (eds.), The
1024 Carswell Structure Uranium Deposits Saskatchewan. Geological Association of Canada
1025 Special Paper 29, pp. 213–223
1026 Pagel M, Ahamdach N (1995) Etude des inclusions fluides dans les quartz des gisements d'uranium
1027 de l'Athabasca et du Thelon (Canada). CREGU internal report, 9 p
1028 Piqué A, Canals A, Grandia F, Banks DA (2008) Mesozoic fluorite veins in NE Spain record
1029 regional base metal-rich brine circulation through basin and basement during extensional
1030 events. Chem Geol 257:139–152
1031 Pluta I, Zuber A (1995) Origin of brines in the Upper Silesian Coal Basin (Poland) inferred from
1032 stable isotope and chemical data. Appl Geochem 10:447–460
1033 Poty B, Pagel M (1988) Fluid inclusions related to uranium deposits: a review. Journal of the
1034 Geological Society of London 145:157–162
1035 Quirt D (2003) Athabasca unconformity-type uranium deposits: one type of deposit with many
1036 variations. Proceedings of International Conference Uranium Geochemistry 2003, Nancy,
1037 pp. 309–312
1038 Raffensperger JP, Garven G (1995) The formation of unconformity-type uranium ore deposits 2.
1039 Coupled hydrochemical modeling. Am J Sci 295:639–696
1040 Ramaekers P, Jefferson CW, Yeo GM, Collier B, Long DG, Catuneanu O, Bernier S, Kupsch B,
1041 Post R, Drever G, McHardy S, Jircka D, Cutts C, Wheatley K (2007) Revised geological
1042 map and stratigraphy of the Athabasca Group, Saskatchewan and Alberta. Geological
1043 Survey of Canada Bulletin 588:155–191

1044 Richard A, Pettke T, Cathelineau M, Boiron MC, Mercadier J, Cuney M, Derome D (2010) Brine-
1045 rock interaction in the Athabasca basement (McArthur River U deposit, Canada):
1046 consequences for fluid chemistry and uranium uptake. Terra Nova 22:303–308
1047 Richard A, Banks DA, Mercadier J, Boiron MC, Cuney M, Cathelineau M (2011) An evaporated
1048 seawater origin for the ore-forming brines in unconformity-related uranium deposits
1049 (Athabasca Basin, Canada): Cl/Br and δ^{37}Cl study of fluid inclusions. Geochim Cosmochim
1050 Acta 75:2792–2810
1051 Richard A, Rozsypal C, Mercadier J, Banks DA, Cuney M, Boiron MC, Cathelineau M (2012)
1052 Giant uranium deposits formed from exceptionally uranium-rich acidic brines. Nat Geosci
1053 5:142–146
1054 Richard A, Cauzid J, Cathelineau M, Boiron MC, Mercadier J, Cuney M (2013a) Synchrotron-XRF
1055 and XANES investigation of uranium speciation and element distribution in fluid
1056 inclusions from unconformity-related uranium deposits. Geofluids 13:101–111
1057 Richard A, Boulvais P, Mercadier J, Boiron MC, Cathelineau M, Cuney M, France-Lanord C
1058 (2013b). From evaporated seawater to uranium-mineralizing brines: Isotopic and trace
1059 element study of quartz-dolomite veins in the Athabasca system. Geochim Cosmochim
1060 Acta 113:38–59
1061 Richard A, Kendrick MA, Cathelineau M (2014) Noble gases (Ar, Kr, Xe) and halogens (Cl, Br, I)
1062 in fluid inclusions from the Athabasca Basin (Canada): Implications for unconformity-
1063 related U deposits. Precambrian Res 247:110–125
1064 Ruzicka V (1989) Monometallic and polymetallic deposits associated with sub-Athabasca
1065 unconformity in Saskatchewan. Geological Survey of Canada Paper 1–C, 67–79
1066 Sánchez V, Vindel E, Martin-Crespo T, Corbella M, Cardellach E, Banks DA (2009) Sources and
1067 composition of fluids associated with fluorite deposits of Asturias (N Spain). Geofluids
1068 9:338–355

1069 Scott R, Chi G, Bosman SA (2011) A petrographic and fluid inclusion study of the Athabasca
1070 Group sandstones from Rumpel Lake drill core, Athabasca Basin, northern Saskatchewan.
1071 In: Summary of investigations 2011, Volume 2. Saskatchewan Geological Survey,
1072 Saskatchewan Ministry of Energy and Resources, Miscellaneous Report 2011-4.2 paper A-
1073 5, 10p
1074 Shelton KL, Burstein IB, Hagni RD, Vierrether CB, Grant SK, Hennigh QT, Bradley MF, Brandom
1075 RT (1995) Sulfur isotope evidence for penetration of MVT fluids into igneous basement
1076 rocks, southeast Missouri, USA. Miner Deposita 30:339–350
1077 Shepherd TJ, Chenery SR (1995) Laser ablation ICP-MS elemental analysis of individual fluid
1078 inclusions: An evaluation study. Geochim Cosmochim Acta 59:3997–4007
1079 Steele-MacInnis M, Bodnar RJ, Naden J (2011) Numerical model to determine the composition of
1080 H_2O-NaCl-$CaCl_2$ fluid inclusions based on microthermometric and microanalytical data.
1081 Geochim Cosmochim Acta 75:21–40
1082 Stoffell B, Wilkinson JJ, Jeffries TE (2004) Metal transport and deposition in hydrothermal veins
1083 revealed by 213nm UV laser ablation microanalysis of single fluid inclusions. Am J Sci
1084 304:533–557
1085 Stoffell B, Appold MS, Wilkinson JJ, McClean NA, Jeffries TE (2008) Geochemistry and evolution
1086 of Mississippi Valley-type mineralizing brines from the Tri-State and Northern Arkansas
1087 districts determined by LA-ICP-MS microanalysis of fluid Inclusions. Econ Geol 103:1411–
1088 1435
1089 Stueber AM, Walter LM (1991) Origin and chemical evolution of formation waters from Silurian-
1090 Devonian strata in the Illinois basin, USA. Geochim Cosmochim Acta 55:309–325
1091 Sverjensky DA (1984) Oil field brines as ore-forming solutions. Econ Geol 79:23–37
1092 Sverjensky DA (1989) Chemical evolution of basinal brines that formed sediment-hosted Cu-Pb-Zn
1093 deposits. In: Boyle RW, Brown AC, Jefferson CJ, Jowett EC, Kirkham RV (eds.), Sediment

1094 Hosted Stratiform Copper deposits. Geological Association of Canada Special Paper
1095 36:127–134
1096 Swarbrick RE, Osborne MJ (1997) Mechanisms for generating overpressure in sedimentary basins:
1097 A reevaluation. Am Assoc Petr Geol B 81:1023–1041
1098 Vanko DA, Bodnar RJ, Sterner SM (1988) Synthetic fluid inclusions: VIII. Vapor-saturated halite
1099 solubility in part of the system NaCl-$CaCl_2$-H_2O, with application to fluid inclusions from
1100 oceanic hydrothermal systems. Geochim Cosmochim Acta 52:2451–2456
1101 Warren JK (1997) Evaporites, brines and base metals: Fluids, flow and 'the evaporite that was'. Aust
1102 J Earth Sci 44:149–183
1103 Wilkinson JJ, Everett CE, Boyce AJ, Gleeson SA, Rye DM (2005) Intracratonic crustal seawater
1104 circulation and the genesis of subseafloor zinc-lead mineralization in the Irish orefield.
1105 Geology 33:805–808
1106 Wilkinson JJ, Stoffell B, Wilkinson CC, Jeffries TE, Appold MS (2009) Anomalously metal-rich
1107 fluids form hydrothermal ore deposits. Science 323:764–767
1108 Wilson MR, Kyser TK (1987) Stable isotope geochemistry of alteration associated with the Key
1109 Lake uranium deposit, Canada. Econ Geol 82:1540–1557
1110 Wilson MR, Kyser TK, Mehnert HH, Hoeve J (1987) Changes in the H-O-Ar isotope composition
1111 of clays during retrograde alteration. Geochim Cosmochim Acta 51:869–878
1112 Worden RH, Manning DAC, Bottrell SH (2006) Multiple generations of high salinity formation
1113 water in the Triassic Sherwood Sandstone: Wytch Farm oilfield, onshore UK. Appl Geochem
1114 21:455–475
1115 Yardley BWD (2005) 100th Anniversary Special Paper: Metal concentrations in crustal fluids and
1116 their relationship to ore formation. Econ Geol 100:613–632

Zhang YG, Frantz JD.(1987) Determination of the homogenization temperatures and densities of supercritical fluids in the system NaCl-KCl-$CaCl_2$-H_2O using synthetic fluid inclusions. Chem Geol 64:335–350

Zwart EW, Touret JLR (1994) Melting behavior and composition of aqueous fluid inclusions in fluorite and calcite: applications within the system H_2O-$CaCl_2$-NaCl. Eur J Mineral 6:773–786

Table captions

Table 1: Fluid inclusion nomenclature and summary fluid inclusion data for the McArthur River deposit, after Derome et al. (2005) and Richard et al. (2010). LA-ICP-MS: laser ablation-inductively coupled plasma-mass spectrometry; hyd.: hydrohalite; Te: eutectic melting; Tm ice: ice melting; Tm hyd: hydrohalite melting; Ts NaCl: halite dissolution; Th: homogenization to the vapor phase; LIBS: laser-induced breakdown spectroscopy. Lw' and Lwh' inclusions frequently fail to nucleate any ice upon cooling, and only observed Tm ice ranges are reported.

Table 2: Summary of fluid inclusion types previously described in the Athabasca Basin and Basement. Fluid inclusion microthermometric data from previous studies were compiled and fluid inclusions classified based on the nomenclature used in Derome et al. (2005), Richard et al. (2010) and Mercadier et al. (2010); see Section "Fluid inclusion nomenclature and previous studies" for details. Only primary or pseudosecondary fluid inclusions are considered here except for secondary fluid inclusions in magmatic and metamorphic quartz from basement rocks. References are as follows: 1: Derome et al. 2005; 2: Richard et al. 2010; 3: Kotzer and Kyser 1995; 4: Pagel and Ahamdach 1995; 5: Mercadier et al. 2010; 6:

1142 Pagel et al. 1980; 7: Freiberger et al. 2003; 8: Lawler and Crawford 1982; 9: Pagel 1975a;
1143 10: Pagel 1975b; 11: Pagel and Ahamdach 1995; 12: Scott et al. 2011; 13: Beshears 2010;
1144 14: Poty and Pagel 1988.
1145
1146 **Figure captions**
1147
1148 Fig. 1: (A) Simplified geological map of the Athabasca Basin and Basement, Canada, modified
1149 from Jefferson et al. (2007). Circles indicate the locations of the main uranium deposits
1150 (including those mentioned in Table 3 with the exception of Rumpel Lake, where only
1151 typical alteration is described but no mineralization. Large red circles represent the uranium
1152 deposits studied in this work. Basement domains are identified by different shades of grey.
1153 TMZ: Thelon magmatic zone; WMTZ: Wollaston Mudjatik transition zone; VRSZ: Virgin
1154 River shear zone; BLSZ: Black Lake shear zone. The Snowbird Tectonic Zone separates the
1155 Rae Subprovince in the west from the Hearne Subprovince in the east. (B) Simplified
1156 mineral paragenesis for unconformity-related U deposits in the Athabasca Basin and
1157 Basement. Alteration types (E: early diagenetic, hydrothermal and late meteoric) are
1158 indicated. Diag.: diagenetic. Modified from Kotzer and Kyser (1995), Derome et al. (2005)
1159 and Kyser and Cuney (2008) for early diagenetic and hydrothermal events, and Mercadier et
1160 al. (2011a) for late meteoric events.
1161
1162 Fig. 2: Examples of fluid-inclusion-hosting quartz and dolomite veins studied in this work. (A)
1163 Hematite-dolomite vein cross-cutting a biotite-rich gneiss (sample H1935-8, Eagle Point).
1164 (B) Quartz ± hematite veins cross-cutting a hematite-rich gneiss (sample ERC5-922.0, Shea
1165 Creek). (C) Quartz-dolomite vein cross-cutting a hematite-rich gneiss (sample RBL2Qz,
1166 Rabbit Lake). (D) Quartz-dolomite vein cross-cutting “bleached” (illite-chlorite-dravite

alteration) gneiss (sample CX52-1, Millennium). (E) Quartz vein cross-cutting "bleached" gneiss (sample P48-5, P-Patch). (F) Primary two-phase (liquid + vapor) fluid inclusions aligned along a dolomite growth band (highlighted by white dashed lines). (G) Cluster of primary and pseudosecondary two-phase (liquid + vapor) fluid inclusions. Pseudosecondary fluid inclusions planes are highlighted by black dashed lines. A quartz growth band is highlighted by a white dashed line. In such cases, primary and pseudosecondary inclusions are petrographically nearly indistinguishable. (H) Three-phase (liquid-vapor-halite) primary inclusion in quartz, showing negative crystal shape. Further illustration of fluid inclusions and quartz-dolomite veins, breccias and cements from McArthur River, Rabbit Lake, P-Patch and Millennium, can be found in Pagel et al. 1980; Kotzer and Kyser 1995; Derome et al. 2005; Mercadier et al. 2010; Beshears 2010; Richard et al. 2010, 2011, 2012).

Fig. 3: Fluid inclusion compositions in the ternary H_2O-NaCl-$CaCl_2$ system from microthermometric data for the Rabbit Lake (A), Eagle Point (B), Shea Creek (C), P-Patch (D) and Millennium (E) deposits, together with data for the McArthur River deposit (F) from Derome et al. (2005). (G) Compilation of data from all deposits. (H) Possible compositional fields for the different fluid-inclusion types. Ternary diagrams have been modified from Vanko et al. (1988).

Fig. 4: Ice melting temperature (Tm ice) - Homogenization temperature (Th) relationships of the quartz-hosted Athabasca fluid inclusions for the P-Patch, Eagle Point, Shea Creek and Rabbit Lake deposits, together with data for the McArthur River deposit from Derome et al. (2005).

Fig. 5: Ice melting temperature (Tm ice) - Homogenization temperature (Th) relationships of the dolomite-hosted Athabasca fluid inclusions for the Rabbit Lake, Eagle Point and P-Patch deposits.

Fig. 6: Homogenization temperature (Th) - Halite dissolution temperature (Ts NaCl) - phase volume relationships of the Athabasca fluid inclusions for the P-Patch, Eagle Point, Shea Creek and Rabbit Lake deposits, together with data for the McArthur River deposit from Derome et al. (2005). (A) Ts NaCl vs Th for quartz- and dolomite-hosted fluid inclusions. Note that Lwh' inclusions were not found in dolomite. (B) Distribution of Δ(Ts NaCl - Th) values as a function of the volumetric relationship between NaCl and the vapor phase in the fluid inclusions. V(vap): volume of the vapor phase; V(NaCl): volume of the NaCl phase.

Fig. 7: LA-ICP-MS data for individual quartz-hosted fluid inclusions from the Rabbit Lake, P-Patch, Eagle Point, Millennium and McArthur River deposits. Data for McArthur River after Richard et al. (2010). Stars indicate the possible composition of epsomite-saturated evaporated seawater from which the NaCl-rich and $CaCl_2$-rich brines originated (see Section "Origin and behavior of major solutes and metals" for details). Red stars ($MgSO_4$ seas) after Fontes and Matray (1993). Blue stars ($CaCl_2$ seas) after Lowenstein and Timofeef (2008). Arrows indicate the expected directions of compositional shifts for the following reactions: Mix. with hal.-diss. brine: mixing with halite-dissolution brine; Dol.: dolomitization of calcite; Alb. Pl.: albitization of plagioclase; Alb. KFs.: Albitization of K-feldspar; Mg-alt.: Mg alteration (sudoite, dravite).

Fig. 8: Ranges of element concentrations for the NaCl-rich brine and $CaCl_2$-rich brine end-members from LA-ICP-MS data. The NaCl-rich brine end-member is defined by fluid inclusions with Na > 80000 ppm. The $CaCl_2$-rich brine end-member is defined by fluid inclusions with Na <

30000 ppm. Boxplots show 10^{th} and 90^{th} percentiles (whiskers), 25^{th} and 75^{th} percentiles (box edges) and the median (inner bar).

Fig. 9: Possible P-T reconstruction of the Athabasca brines under static geothermal gradient condition. Representative isochores have been drawn from the most representative range of homogenization temperatures (Th) in both quartz and dolomite. The possible P-T field for the NaCl-rich brine end-member (i.e. before mixing) is ~180 ± 30°C and ~800 ± 400 bars. The possible P-T field for the $CaCl_2$-rich brine end-member (i.e. before mixing) is ~120 ± 30°C and ~600 ± 300 bars). The hydrostatic and lithostatic pressures at 3 and 6 km depth are reported as well as the hydrostatic and lithostatic gradients calculated for thermal gradients of 30°, 35°, and 40°C/km.

Fig. 10: Ranges of metal concentrations in sedimentary formation brines (from boreholes, after Carpenter et al. 1974; Kraemer and Kharaka 1986; Kharaka et al. 1987; Banner et al. 1990; Connolly et al. 1990; Stueber and Walter 1991; Land and Macpherson 1992; Pluta and Zuber 1995; Hodge et al. 1996; Hitchon et al. 2001; Aquilina et al. 2002) and ore fluids from basin-hosted base metal (Pb, Zn, Ba) deposits (from LA-ICP-MS analysis of fluid inclusions, after Appold et al. 2004; Stoffell et al. 2004; Bouch et al. 2006; Huizenga et al. 2006; Piqué et al. 2008; Stoffell et al. 2008; Sanchez et al. 2009; Wilkinson et al. 2009; Appold and Wenz 2011) and Athabasca fluid inclusions (this study). Boxplots show 5^{th} and 95^{th} percentiles (symbols), 10^{th} and 90^{th} percentiles (whiskers), 25^{th} and 75^{th} percentiles (box edges) and the median (inner bar). (1) Typical limits of detection for LA-ICP-MS analysis of metals in fluid inclusions. Black solid lines represent the ranges of the highest values for metal concentrations in each of the selected studies. Grey dotted lines represent the lower ranges of metal concentrations in the selected studies.

Figure 1

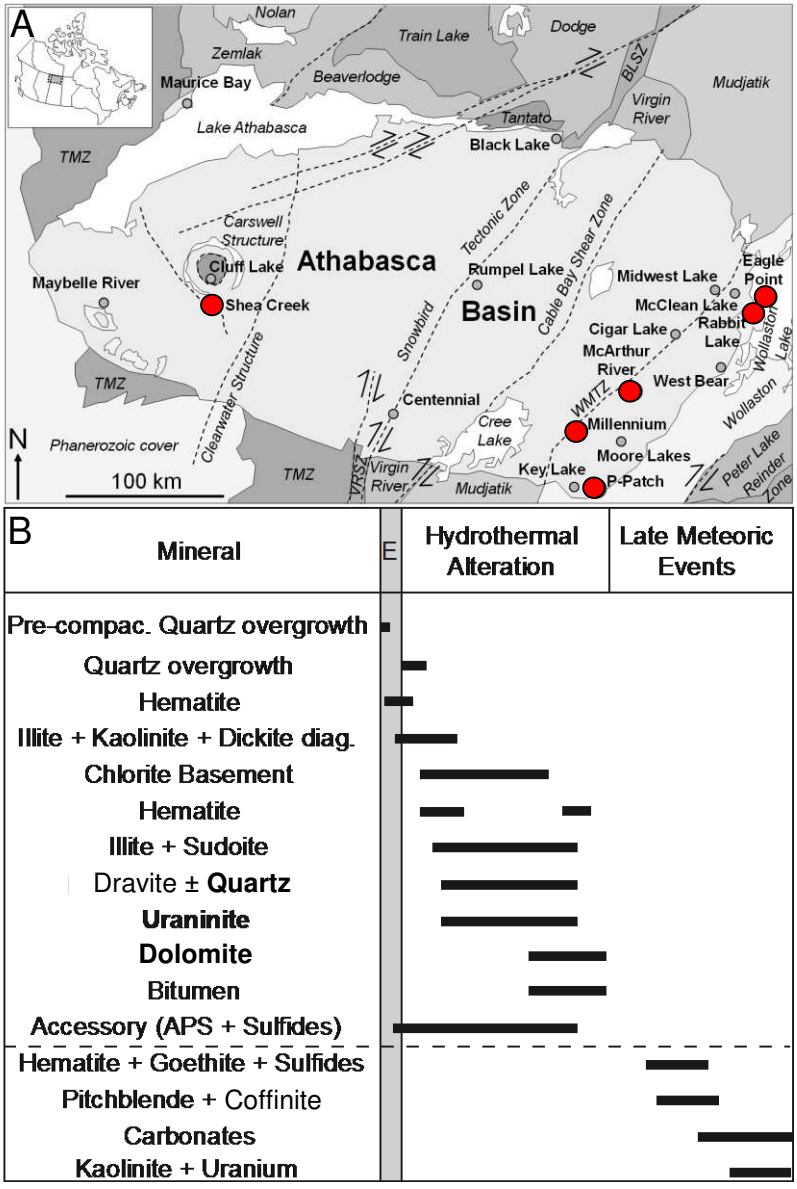

FIGURE 1

Figure 2

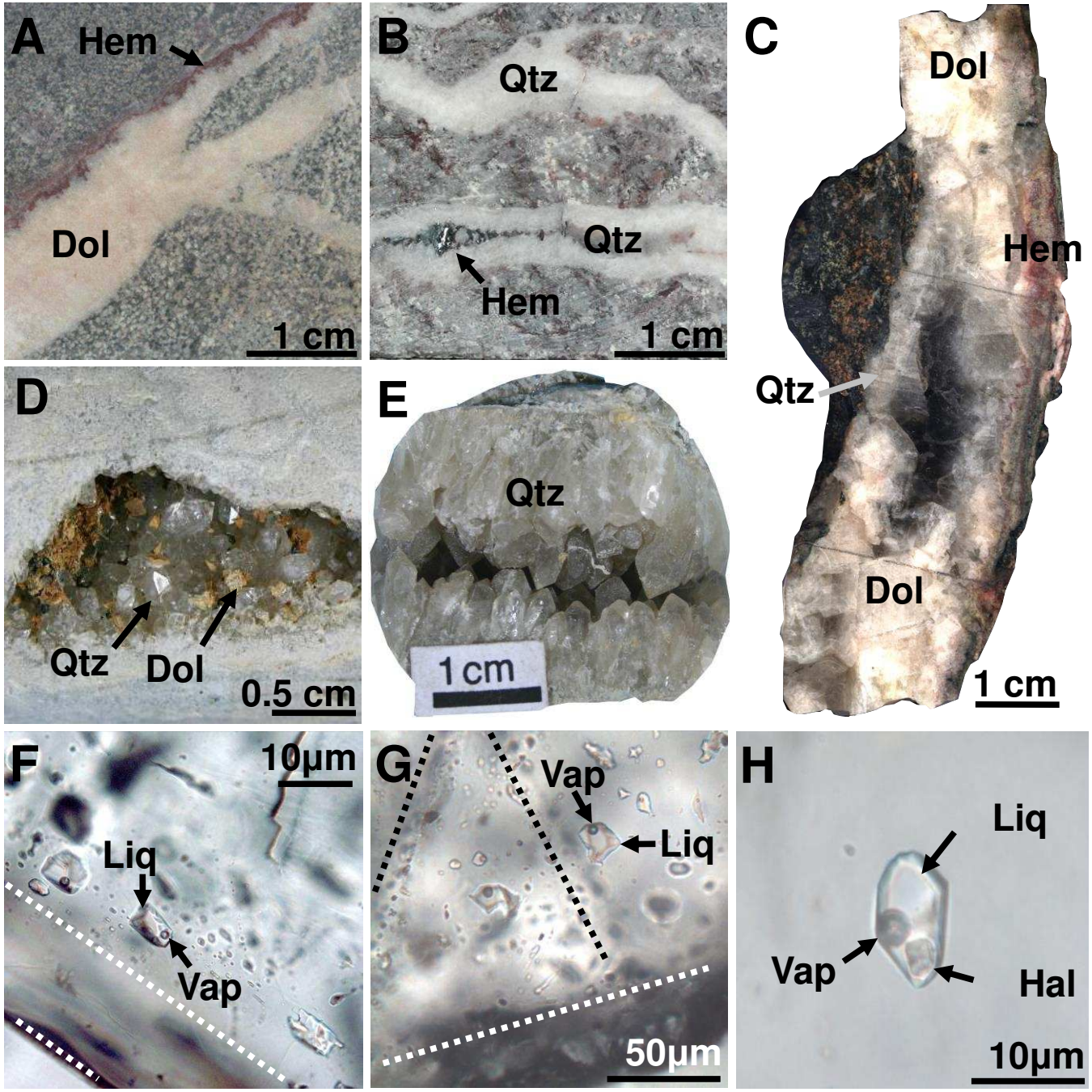

FIGURE 2

Figure 3

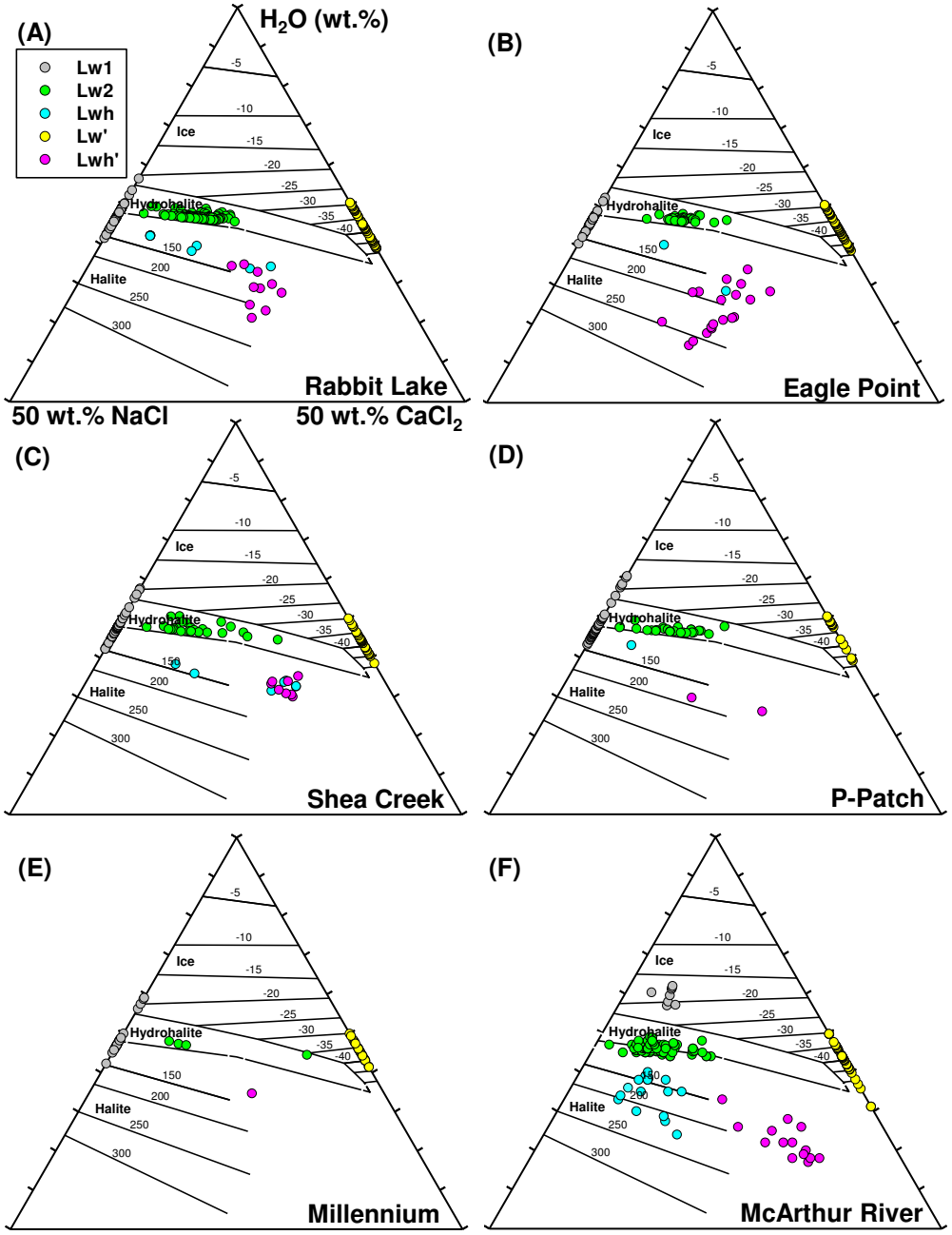

FIGURE 3 (continued on the next page)

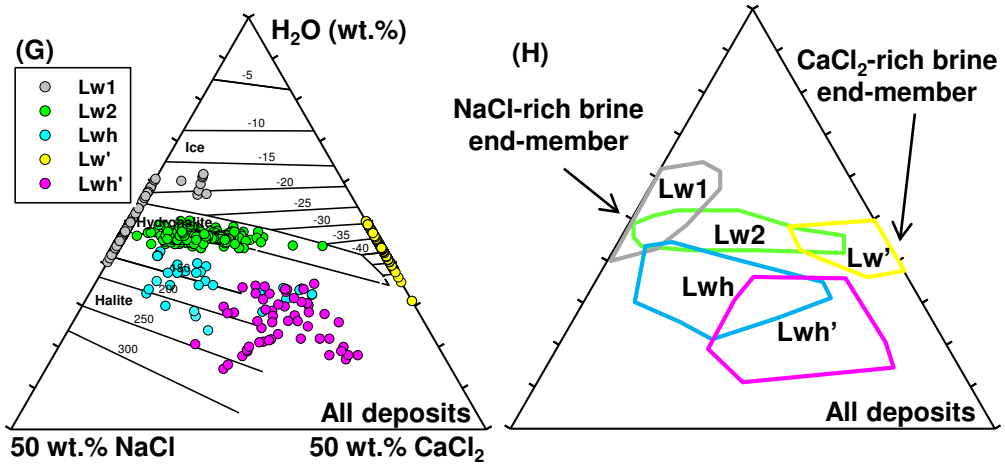
(G)
Lw1
Lw2
Lwh
Lw'
Lwh'
H2O (wt.%)
-5
-10
-15
-20
-25
-30
-35
-40
Ice
Hydrohalite
Halite
200
250
300
All deposits
50 wt.% NaCl
50 wt.% CaCl2
(H)
NaCl-rich brine
end-member
CaCl2-rich brine
end-member
Lw1
Lw2
Lw'
Lwh
Lwh'
All deposits

FIGURE 3

Figure 4

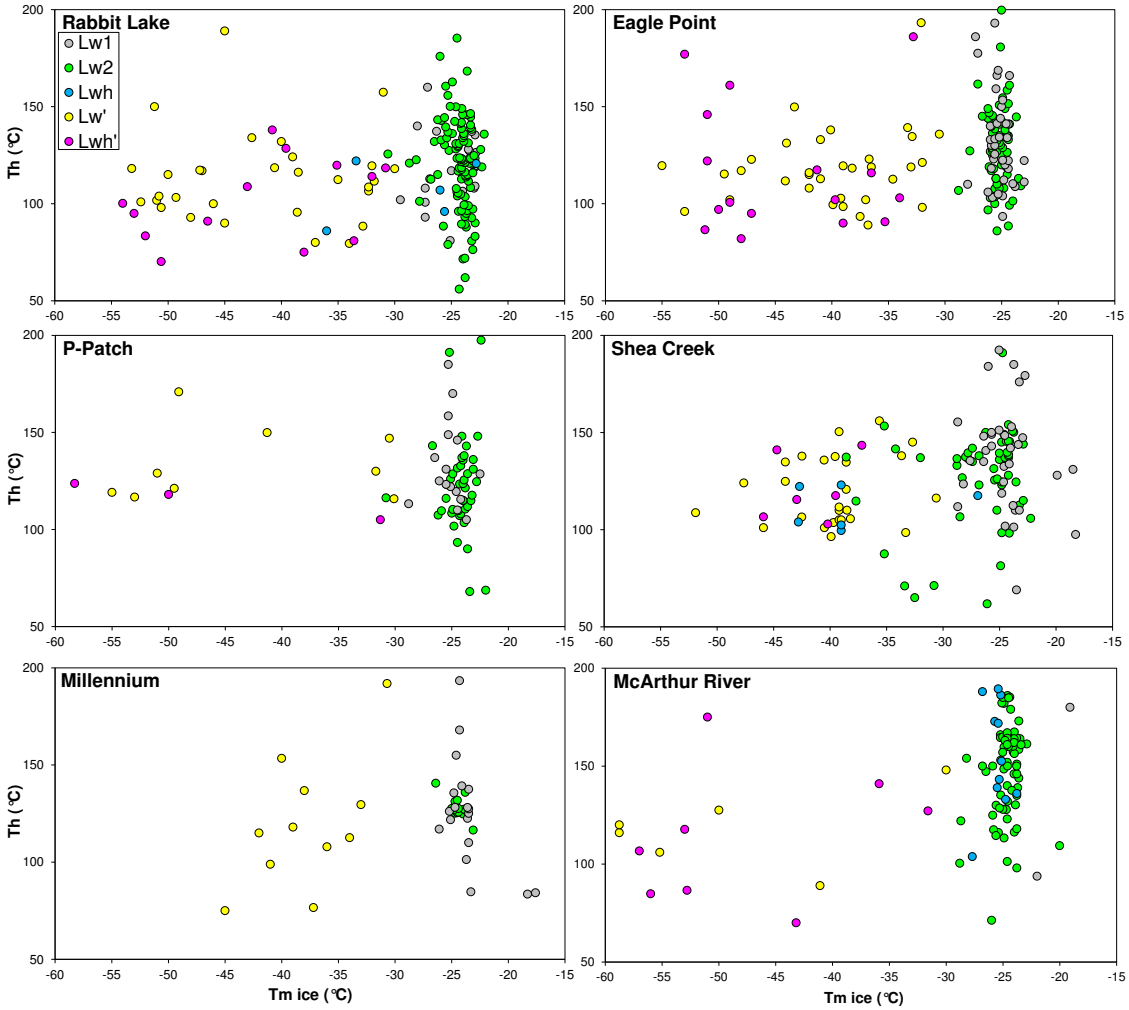

FIGURE 4

Figure 5

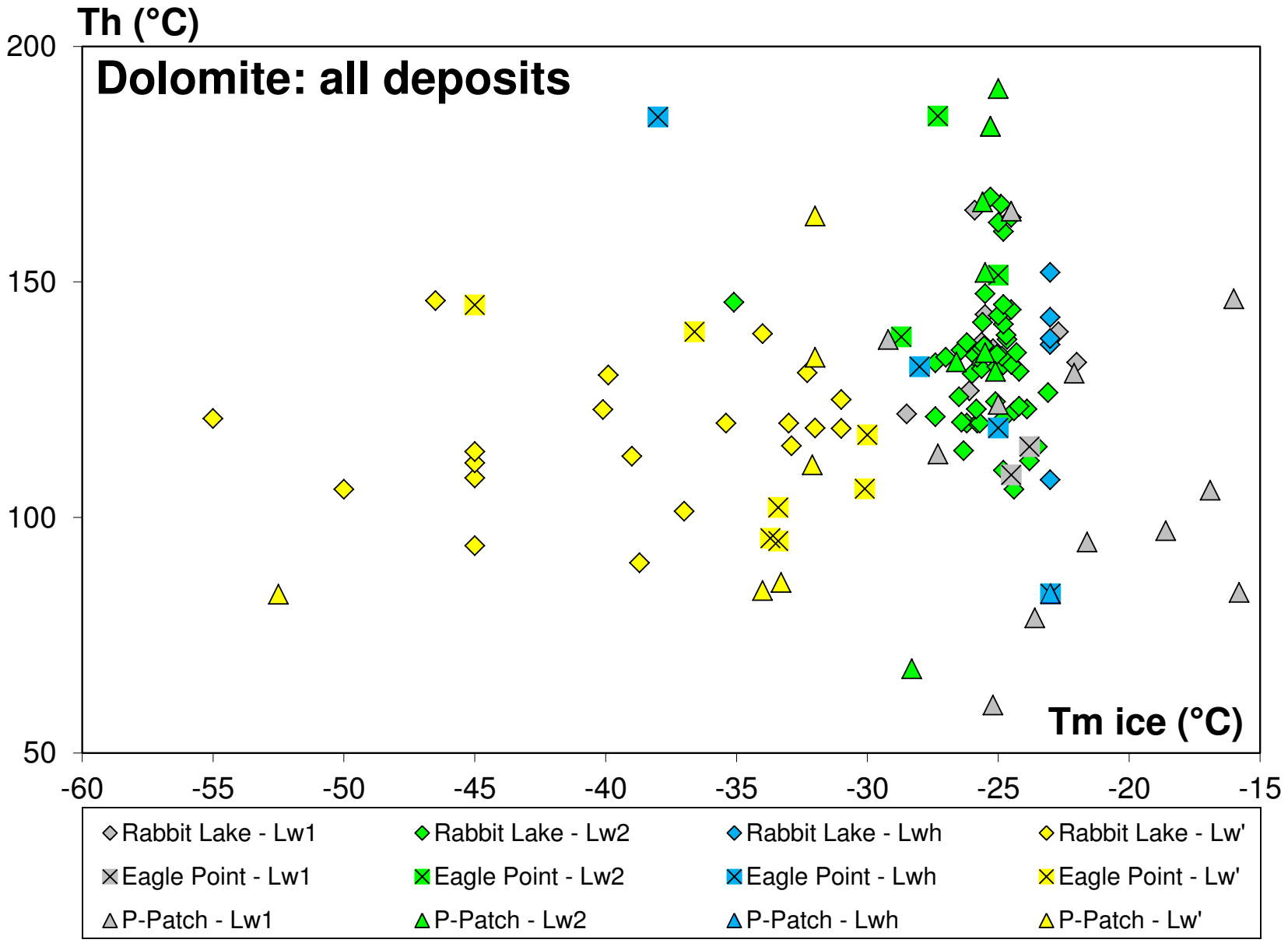

FIGURE 5

Figure 6

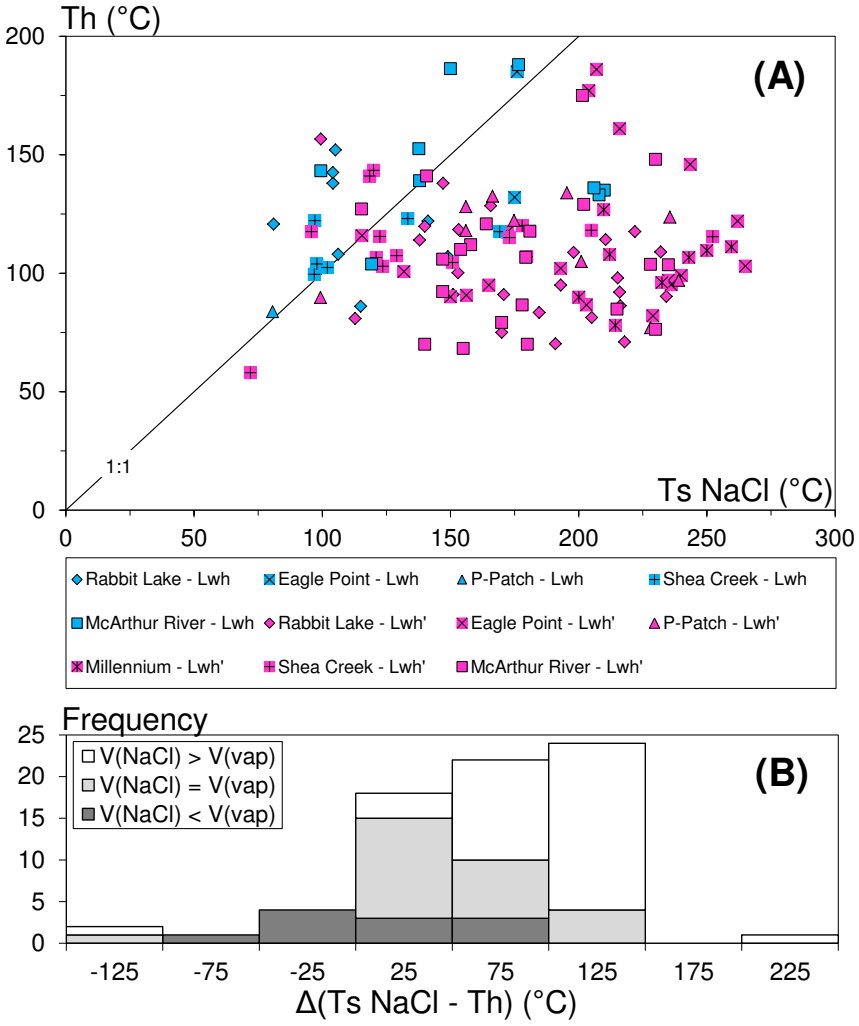

FIGURE 6

Figure 7 (one page)

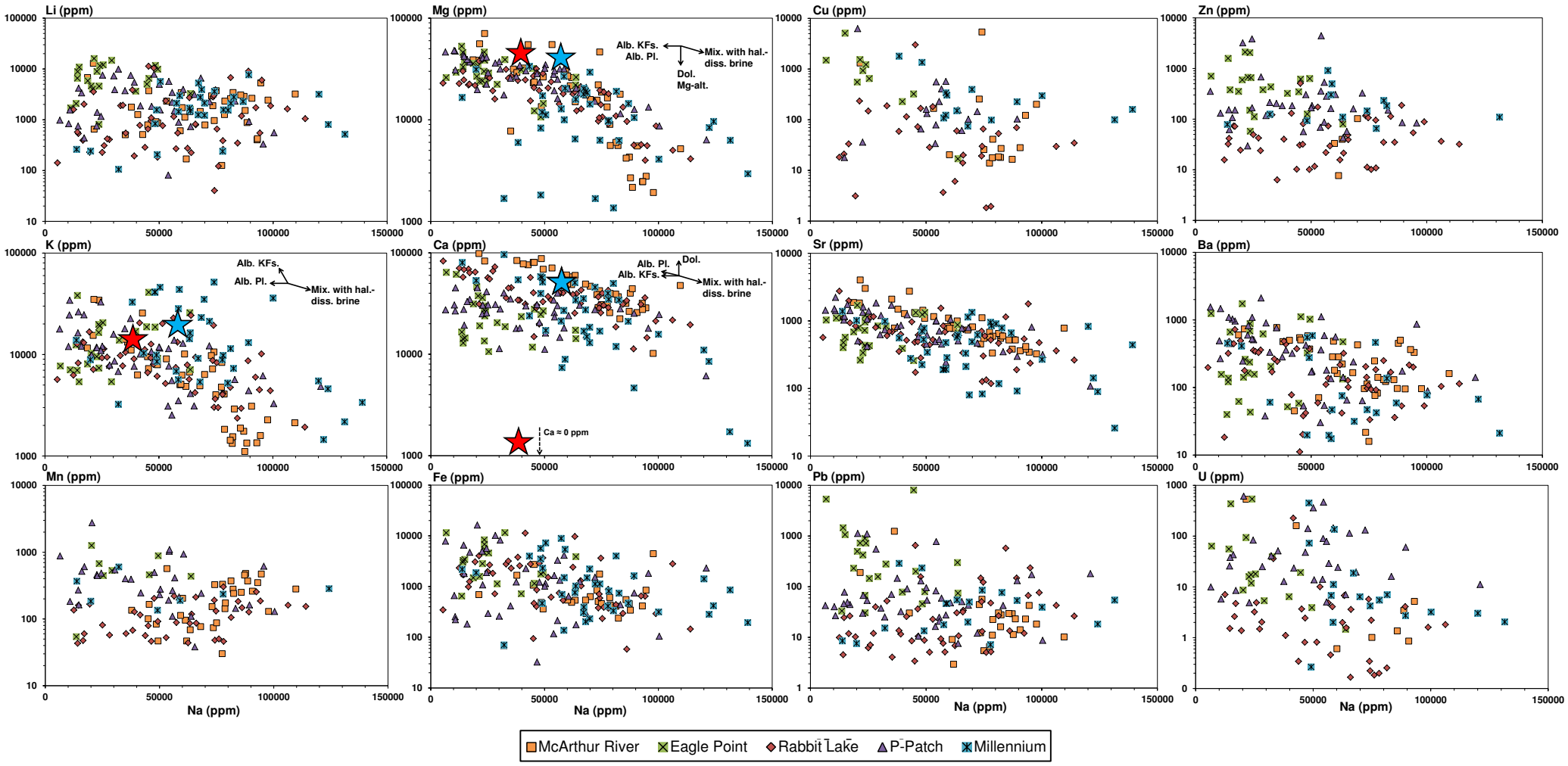

FIGURE 7

Figure 8

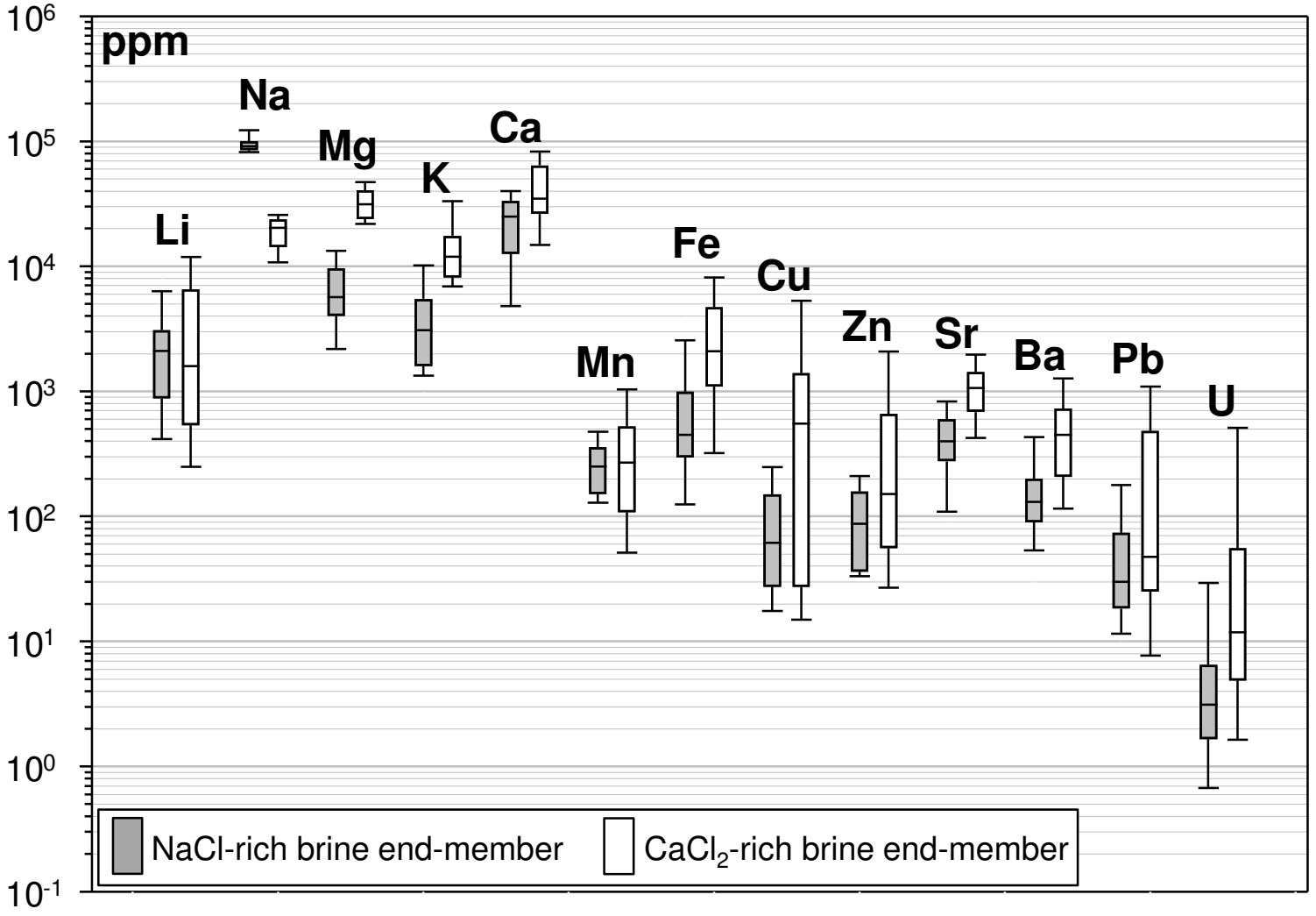

FIGURE 8

Figure 9

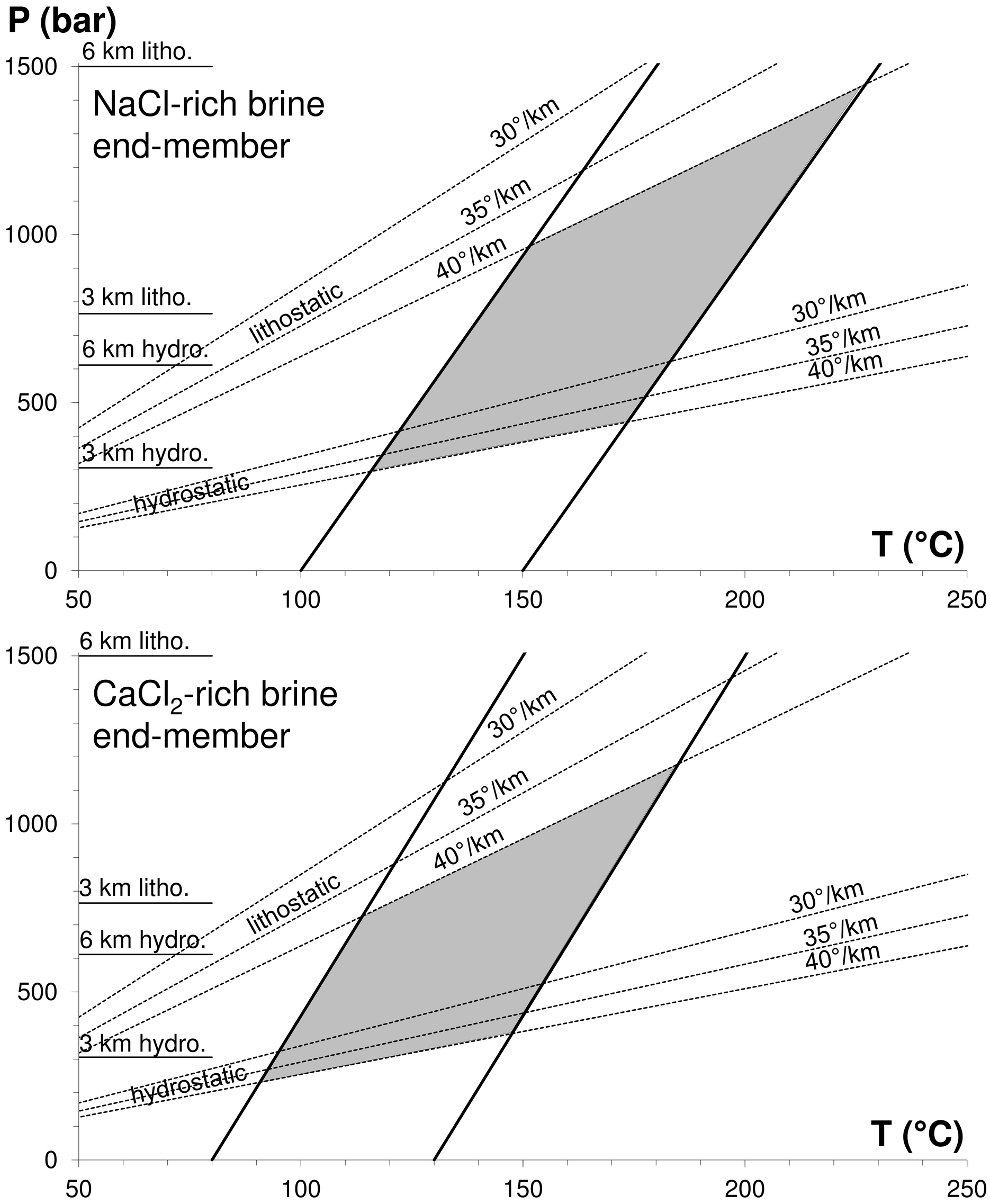

FIGURE 9

Figure 10

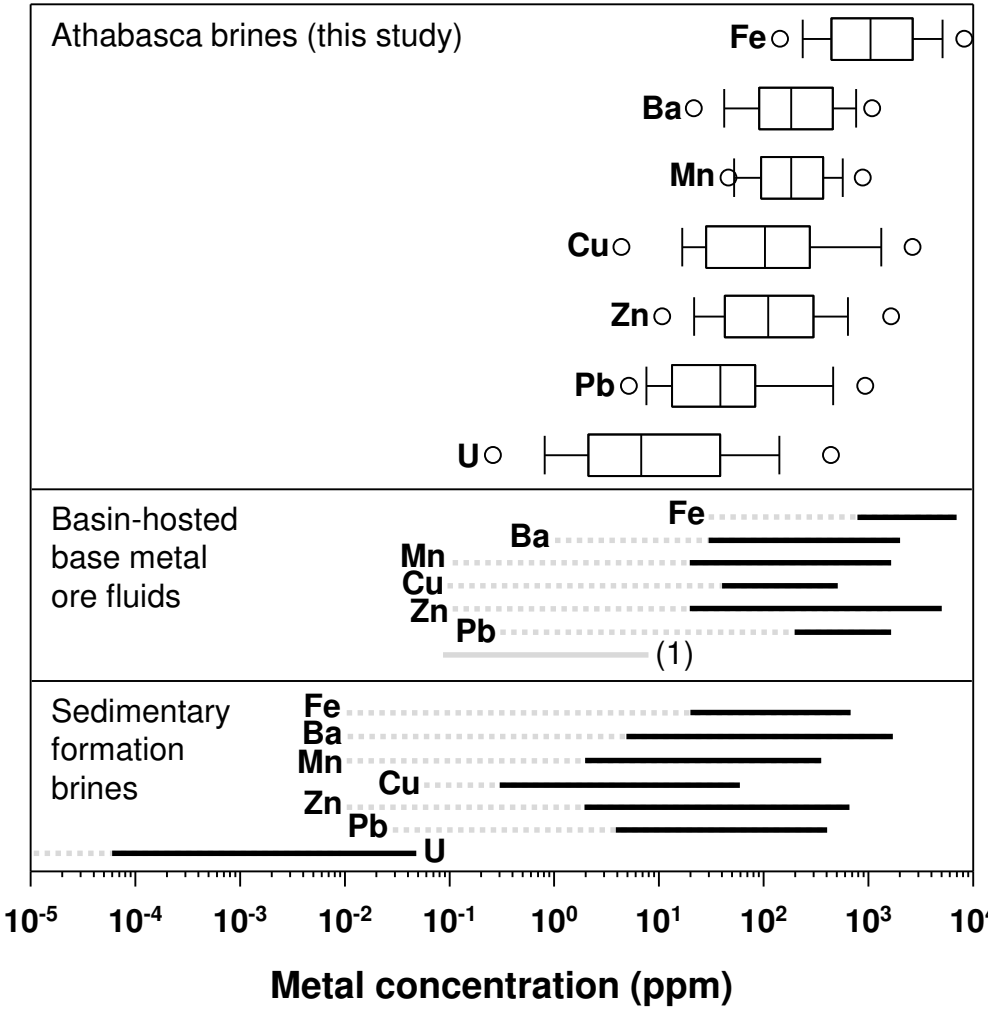

FIGURE 10

Table 1

	NaCl-rich brine			$CaCl_2$-rich brine	
	End-member compositions from LA-ICP-MS				
Na (ppm)	80000 to 100000			20000 to 40000	
Ca (ppm)	20000 to 50000			80000 to 130000	
Mg (ppm)	2000 to 10000			30000 to 70000	
K (ppm)	1000 to 5000			10000 to 35000	
U (ppm)	100 to 500			1 to 10	
	Microthermometric characteristics				
Fluid inclusion types	Lw1	Lw2	Lwh	Lw'	Lwh'
NaCl at room T°	no	no	yes	no	yes
Last phase to melt	ice	hyd.	hyd.	ice	ice
Te (°C)	-75 to -50	-75 to -50	-75 to -50	-75 to -60	-75 to -60
Tm ice (°C)	-25 to -11.2	-28.8 to -21	-27.7 to -24	-60 to -30	-58 to -36
Tm hyd (°C)	-	-7 to 21.9	-3.2 to 19.2	-	-
Ts NaCl (°C)	-	-	99.5 to 208	-	115 to 235
Th (°C) mode	165	165	135	115	115
	Composition from microthermometry, Raman and LIBS				
	Lw1	Lw2	Lwh	Lw'	Lwh'
Cl (molal)	3 to 4.5	5.5 to 6.5	6.5	6	6.5
Na/Ca (mole)	4.6	3 to 7.7	3.8	0.5	0.8
Ca/Mg (mole)	1	1 to 17.9	-	1.5	1.7
wt.% NaCl	14	22 to 24	25	5	8
wt.% $CaCl_2$	6	6 to 12	13	20	19
wt.% $MgCl_2$	4	0 to 0.9	0	11.5	9.5

Table 2

Locality	Reference	Sample description	Fluid inclusion types				
			NaCl-rich brine			$CaCl_2$-rich brine	
			Lw1	Lw2	Lwh	Lw'	Lwh'
McArthur River	1, 2, 3, 4	Quartz overgrowths in sandstones	yes			yes	yes
		Quartz cementing veins and breccias	yes	yes	yes	yes	yes
P-Patch	5	Magmatic and metamorphic quartz	yes	yes	yes	yes	yes
Rabbit Lake	6	Quartz cementing veins and breccias			yes		yes
		Dolomite cementing veins and breccias		yes	yes		
Shea Creek	7	Magmatic and metamorphic quartz	yes				
Midwest	8	Unknown			yes		
Eagle Point	3	Quartz cementing veins and breccias			yes		yes
Cluff Lake	9, 10	Quartz overgrowths in sandstones	yes		yes	yes	yes
Sue C - McClean	11	Quartz cementing veins and breccias	yes		yes	yes	yes
Rumpel Lake	9, 10, 12	Quartz overgrowths in sandstones	yes		yes	yes	yes
Millennium	13	Quartz cementing veins and breccias	yes				
		Metamorphic quartz	yes				
Key Lake	14	Quartz overgrowths in sandstones			yes		

Electronic Supplementary Material

Click here to download Supplementary Material: Richard et al. Electronic Supplementary Material.pdf